FISFVIER

Contents lists available at ScienceDirect

## Journal of Computational Physics

journal homepage: www.elsevier.com/locate/jcp





# A first-order computational algorithm for reaction-diffusion type equations via primal-dual hybrid gradient method

Shu Liu<sup>a</sup>, Siting Liu<sup>a</sup>, Stanley Osher<sup>a</sup>, Wuchen Li<sup>b,\*</sup>

- a Department of Mathematics, University of California, Los Angeles, United States of America
- b Department of Mathematics, University of South Carolina, Columbia, SC, United States of America

#### ARTICLE INFO

## Keywords:

Primal-dual hybrid gradient algorithm Reaction-diffusion equations First order optimization algorithm Implicit finite difference schemes Preconditioners

#### ABSTRACT

We propose an easy-to-implement iterative method for resolving the implicit (or semi-implicit) schemes arising in solving reaction-diffusion (RD) type equations. We formulate the nonlinear time implicit scheme as a min-max saddle point problem and then apply the primal-dual hybrid gradient (PDHG) method. Suitable precondition matrices are applied to the PDHG method to accelerate the convergence of algorithms under different circumstances. Furthermore, our method is applicable to various discrete numerical schemes with high flexibility. From various numerical examples tested in this paper, the proposed method converges properly and can efficiently produce numerical solutions with sufficient accuracy.

#### 1. Introduction

Reaction-diffusion (RD) equations (systems) have broad applications in many scientific and engineering areas. In material science, the phase-field model is described by typical RD-type equations known as Allen-Cahn [1] or Cahn-Hilliard equations [5]. They are used to model the development of microstructures in a mixture of two or more materials or phases over time; In chemistry, RD systems are used to depict the reaction and diffusion phenomena of chemical species in which a variety of patterns are produced [39,41]; RD systems are also ubiquitous tools in biology: They are widely used for modeling morphogenesis [12], as well as the evolution of species distribution in ecology system [36]. In recent years, researchers also found that RD equations are useful in modeling and predicting crimes [46].

Reaction-diffusion (RD) equations are nonlinear parabolic partial differential equations possessing the following general form

$$\frac{\partial u(x,t)}{\partial t} = \mathcal{L}u(x,t) + \mathcal{R}u(x,t) \quad \text{on } \Omega \subset \mathbb{R}^d,$$
with initial condition  $u(\cdot,0) = u_0$ ,

where  $\mathcal{L}$  is a certain non-positive definite differential operator associated with the diffusion process. For example,  $\mathcal{L}$  can be taken as the Laplace operator  $\Delta$  or negative biharmonic operator  $-\Delta^2$ , or more general operators with variable coefficients;  $\mathcal{R}$  is a nonlinear operator depicting the reaction process. The RD equation is usually equipped with either the Neumann boundary condition if  $\Omega$  is an ordinary region in  $\mathbb{R}^d$ , or the periodic boundary condition if  $\Omega$  is a periodic region  $\mathbb{T}^d$ . We can also extend the RD equation (1) from the 1D function u to multiple dimensional vector function u:

E-mail addresses: shuliu@math.ucla.edu (S. Liu), siting6@math.ucla.edu (S. Liu), sjo@math.ucla.edu (S. Osher), wuchen@mailbox.sc.edu (W. Li).

https://doi.org/10.1016/j.jcp.2024.112753

Received 3 May 2023; Received in revised form 22 November 2023; Accepted 1 January 2024

<sup>\*</sup> Corresponding author.

S. Liu, S. Liu, S. Osher et al.

$$\frac{\partial \boldsymbol{U}(x,t)}{\partial t} = \mathcal{L}\boldsymbol{U}(x,t) + \mathcal{R}\boldsymbol{U}(x,t) \quad \text{on } \Omega \subset \mathbb{R}^d,$$
with initial condition  $\boldsymbol{U}(\cdot,0) = \boldsymbol{U}_0$ .

Equation (2) can also be equipped with either Neumann or periodic boundary conditions. We also call the equation (2) reaction-diffusion system.

In recent decades, numerical methods, including finite difference methods [34,18,25,28,8,13,44,42,43,51,29–31] and finite element methods [25,53,20], have been developed for computing the reaction-diffusion type equations (systems). Several benchmark problems [27,14] have also been introduced to verify the proposed methods' effectiveness.

In order to get rid of the restriction of the Courant–Friedrichs–Lewy (CFL) condition [16] on small time steps, most of the popular numerical schemes designed for solving reaction-diffusion equations (systems) in the aforementioned works of literature are implicit or semi-implicit. It is worth mentioning that the implicit scheme enjoys particular advantages in preserving stability and accuracy compared with other types of semi-implicit or explicit schemes. We refer the readers to [50] and the references therein for some detailed discussions. As one uses implicit schemes for solving RD equations (systems) with nonlinear terms, Newton's method [3] is usually needed for solving the series of nonlinear equations arising from time discretization. However, Newton's method encounters several drawbacks that may affect the performance of the proposed numerical scheme, namely,

- For Newton's method to converge, the initial guess must be in proximity to the exact solution of the nonlinear equation; otherwise, divergence may occur.
- When applying Newton's method to solve RD equations on mesh grids, each iteration involves solving a large-scale linear
  equation with the Jacobian matrix of a specific nonlinear function. Solving such large-scale linear equation for multiple Newton
  iterations could be challenging and time-consuming.

In this paper, we introduce a method based on the Primal-Dual Hybrid Gradient method (PDHG) [54,9,49,15,26] for solving the nonlinear updates arising in the time discretization schemes of RD equations (systems) with satisfying speed and accuracy.

We sketch the proposed method as follows. We briefly illustrate the main idea by considering the following fully implicit, semi-discrete scheme of the RD equation at the *t*-th time step:

$$\frac{u^{t+1} - u^t}{h_t} = \mathcal{L}u^{t+1} + \mathcal{R}u^{t+1}.$$
 (3)

In this case,  $u^t$  is given, and  $h_t > 0$  is a stepsize. We need to solve for  $u^{t+1}$ . Consider the following function  $\mathcal{F}$ 

$$F(u) = u - h_t(\mathcal{L}u + \mathcal{R}u) - u^t. \tag{4}$$

The goal is to solve  $\mathcal{F}(u) = 0$ . If we consider the indicator function  $\iota$  defined as

$$\iota(u) = \begin{cases} 0 & u = 0 \\ +\infty & u \neq 0. \end{cases}$$

Then the nonlinear functional equation  $\mathcal{F}(u) = 0$  is equivalent to the minimization problem

$$\min_{u \in X} \iota(\mathcal{F}(u)),$$

where X is a certain linear functional space for u. Now since  $\iota$  can be treated as the Legendre transform of the constant function 0, i.e.,  $\iota(u) = \sup_{p \in X^*} \{(p,u)\}$  (here  $X^*$  denotes the dual space of X), we can recast the above minimization problem as a min-max saddle point problem as follows

$$\min_{u \in X} \max_{p \in X^*} \{ (p, \mathcal{F}(u)) \}. \tag{5}$$

We denote  $L(u, p) = (p, \mathcal{F}(u))$ . To deal with the saddle problem (5), by leveraging the ideas proposed in the PDHG method, we evolve p, u via the following proximal algorithms with extrapolation on the dual variable p.

$$p_{n+1} = \underset{p \in X^*}{\operatorname{argmin}} \left\{ \frac{\|p - p_n\|_2^2}{2\tau_p} - L(u_n, p) \right\} = p_n + \tau_p \mathcal{F}(u_n), \tag{6}$$

$$\widetilde{p}_{n+1} = p_{n+1} + \omega(p_{n+1} - p_n),$$
 (7)

$$u_{n+1} = \underset{u \in X}{\operatorname{argmin}} \left\{ \frac{\|u - u_n\|_2^2}{2\tau_u} + L(u, \widetilde{p}_{n+1}) \right\} = (\operatorname{Id} + \tau_u(\widetilde{p}_{n+1}, \partial_u \mathcal{F}))^{-1}(u_n). \tag{8}$$

Here the extrapolation coefficient  $\omega > 0$ ,  $\tau_p$ ,  $\tau_u$  are time steps used to evolve u, p. We should remind the reader to distinguish the PDHG time steps  $\tau_p$ ,  $\tau_u$  from the time step  $h_t$  of the reaction-diffusion equation. Recall  $u^{t+1}$  as the solution to  $\mathcal{F}(u) = 0$ , if we further assume that  $\partial_u \mathcal{F}(u)$ , as a linear map from X to  $X^*$ , is injective. Then it is not hard to verify that  $u = u^{t+1}$ , p = 0 is the equilibrium of the above dynamic (6)-(8). Thus, we may anticipate that, by evolving (6), (7), (8),  $u_k$ ,  $p_k$  could converge to the desired equilibrium point  $u^{t+1}$ , 0.

Furthermore, since  $\mathcal{F}$  is usually nonlinear, the inversion in (8) cannot be directly evaluated. To mitigate this, we replace  $L(u, \widetilde{p}_{k+1})$  by its linearization  $\hat{L}(u, \widetilde{p}_{k+1}) = L(u_k, \widetilde{p}_{k+1}) + (\partial_u L(u_k, \widetilde{p}_{k+1}), u - u_k)$  at  $u = u_k$ . Thus the update of  $u_{k+1}$  will have an explicit form

$$u_{k+1} = u_k - \tau_u(\widetilde{p}_{k+1}, \partial_u \mathcal{F}(u_k)). \tag{9}$$

As a result, we can evolve the discrete-time dynamic (6), (7), (9) for approximating the solution  $u^{t+1}$  of the nonlinear equation  $\mathcal{F}(u) = 0$ , and the explicit updating rules will enable us to deal with large-scale computational problems conveniently and efficiently. This work will mainly focus on applying such a PDHG algorithm to solve various types of reaction-diffusion equations (systems) up to satisfying accuracy and efficiency. Based on the discussion and presentation in this paper, our method may serve as a potential alternative to the widely used Newton-type algorithms for time-implicit updates of reaction-diffusion equations for time-implicit schemes.

It is worth mentioning that instead of designing and analyzing new discretization schemes for RD equations, our paper is mainly devoted to a strategy that can efficiently resolve the ready-made scheme. Thus, in our paper, we will omit most of the discussions on the properties of the numerical scheme but focus more on the implementing details and the effectiveness of the proposed PDHG method.

This paper is organized as follows. In section 2, we do a brief review of the related literature. Then, in section 3, we provide a brief introduction to the Primal-Dual Hybrid Gradients method; then we present the details of how we implement the PDHG method to update the finite difference schemes for RD equations (systems). We then provide some existing theoretical results on the convergence of the PDHG method. We demonstrate our numerical examples in section 4. Our numerical experiments cover the well-known Allen-Cahn and Cahn-Hilliard equations; higher-order gradient flow that emerges from functionalized polymer research; RD system known as the Schnakenberg model, which originates from the study of steady chemical patterns; and RD systems involving nonlocal terms depicting the species evolution of wolves and deer. We conclude the work in section 5. Some of the future research directions will also be discussed in section 5.

### 2. Discussion and comparison with the existing literature

Our method is inspired by [32], in which the authors design a similar algorithm for solving conservation laws. Although the motivation for using PDHG to resolve the implicit scheme remains consistent, we clarify that our treatment of using the implicit scheme for the RD-type equation is distinctively motivated by the following two points.

- 1. Solving the RD equations with a large reaction coefficient is of great interest to the research community due to its relation with the geometric flows [40], [35]; on the other hand, many phase field models such as the Cahn-Hilliard equation involve elliptic operators ahead of the nonlinear reaction terms. In both cases, adopting either the explicit or the IMEX schemes may result in unstable numerical results. But implicit schemes work more stably.
- 2. It is known that the time-implicit schemes naturally preserve the dissipation of the free energy associated with the equation. Explicit or IMEX schemes have no guarantee on such important property;

Furthermore, we also point out that the detailed treatments between our method and those mentioned in [32] remain different. This includes the designing of efficient preconditioners, as well as the strategy of step-by-step computation versus computing on multiple time steps.

It is also worth mentioning that introducing damping terms into wave equations to achieve faster stabilization [19] shares similarity with the limiting stepsize version of applying the PDHG method to PDE-solving algorithms. The damped wave equation considered in [19] can be treated as a first-order dynamic on the functional space with a *linear* infinitesimal generator; on the other hand, our treatment (18)-(20) designs a *nonlinear* dynamic to the desired critical point  $(U_*, 0)$ . The nonlinearity of the dynamics leads to the fundamental difference.

In recent research [11], by applying certain coordinate transformations, the authors improve the primitive primal-dual (PD) flows of the saddle point problem

$$\min_{u} \max_{p} f(u) - g(p) + (Bu, p)$$

with linear operator *B*. The exact formulation (8) in [11] shares similarities with our method (18)-(20). However, we should point out that in our case we deal with the saddle problem

$$\min_{u} \max_{p} (F(u), p),$$

where the inner product involves *nonlinear* functional F, and the f, g in [11] degenerate to 0. Such differences make our treatment distinct from [11].

As a follow-up of [11], in [10], the authors propose a splitting method for solving the nonlinear equation  $\mathcal{A}(x) = 0$  with the monotone operator  $\mathcal{A}(x) = \nabla F(x) + \mathcal{N}x$ , where  $\mathcal{N}^{\top} = -\mathcal{N}$  is skew-symmetric. In contrast, our proposed method can deal with a time-dependent root-finding problem, which generally can not be cast into the aforementioned decomposition.

In addition to the previous literature, PDHG methods are also utilized in [49] to solve nonlinear equations in Magnetic resonance imaging (MRI) with theoretical convergence guarantee.

Furthermore, people have applied PDHG or first-order methods to compute time-implicit updates of Wasserstein gradient flows [6] and reaction-diffusions [7,20]. Compared to them, the proposed approach works for general non-gradient flow reaction-diffusion equations (cf. section 4.3, 4.4).

In recent works [52,4], the authors utilize the weak forms of PDEs and deep learning techniques to compute high-dimensional PDEs. The algorithm in [52] can be formulated as a min-max saddle point problem and is directly solved by alternative stochastic gradient descent and ascent method. Furthermore, in [33], [2] and the references therein, the authors introduce Lagrange multipliers to the residual term of PDEs and formulate a saddle point training scheme to improve the computation of Physics-Informed Neural Networks (PINNs). Although our proposed method shares similarities with the aforementioned research. It differs from them in both the saddle point problem formulation and the computational scheme.

#### 3. PDHG method for reaction-diffusion equation

In recent years, the Primal-Dual Hybrid Gradient (PDHG) method [54,53,9] proves to be an efficient algorithm for solving saddle point problems emerging from imaging. This method is iterative and each of its iterations consists of alternative proximal steps together with a suitable extrapolation. We refer the readers to [9] for further details (both theoretical and experimental) of the method.

#### 3.1. PDHG method for updating implicit finite difference schemes

To clearly convey our proposed idea, let us first consider the following reaction-diffusion equation as an illustrative example on 2D periodic region  $\Omega = \mathbb{T}^2$ . We assume  $\Omega$  is square shaped and denote its side length as L.

$$\frac{\partial u(x,t)}{\partial t} = \lambda \Delta u(x,t) + f(u(x,t)), \quad u(x,0) = u_0(x). \tag{10}$$

Here we assume  $\lambda$  is a positive constant coefficient;  $f: \mathbb{R} \to \mathbb{R}$  is the nonlinear function depicting the reaction term. Since we assume  $\Omega$  to be the periodic region, we use periodic boundary conditions (BC) for equation (10).

Although there are numerous pieces of research on designing numerical schemes for RD equations, to demonstrate how our method works, let us narrow down and focus on the implicit one-step finite difference (FD) scheme. Once we have demonstrated how to implement the method to this implicit scheme, such a method can be easily extended to general numerical schemes.

We discretize the time interval [0,T] into  $N_t$  equal subintervals with length  $h_t = T/N_t$ . Suppose we discretize each side of the region  $\Omega$  into  $N_x$  subintervals with space stepsize  $h_x = L/N_x$ , we choose the central difference scheme to discretize the Laplace operator  $\Delta$ . We denote the discrete Laplace operator with the periodic boundary condition as  $\operatorname{Lap}_{h_x}^P$  which is an  $N_x^2 \times N_x^2$  block-circulant matrix possessing the following form

$$\operatorname{Lap}_{h_x}^{\mathrm{P}} = \frac{1}{h_x^2} \begin{bmatrix} L & I & & & I \\ I & L & I & & & \\ & \ddots & \ddots & \ddots & \\ & & I & L & I \\ I & & & I & L \end{bmatrix}_{N_x \times N_x \text{blocks}} \qquad L = \begin{bmatrix} -4 & 1 & & & 1 \\ 1 & -4 & 1 & & \\ & \ddots & \ddots & \ddots & \\ & & 1 & -4 & 1 \\ 1 & & & 1 & -4 \end{bmatrix}_{N_x \times N_x}.$$

Here I is the  $N_x$  by  $N_x$  identity matrix. We denote  $U^k \in \mathbb{R}^{N_x^2}$  as the numerical solution of (10) at the kth time step. We vectorize the  $N_x \times N_x$  square array along the column to form the 1D vector  $U^k$ . That is, for  $l = i \cdot N_x + j$  with  $1 \le i \le N_x$  and  $1 \le j \le N_x$ ,  $U_l^k$  is the numerical approximation of  $u((j-1)h_x, (i-1)h_x, kh_l)$ .

Now the implicit one-step FD scheme for (10) is cast as

$$U^{k+1} - U^k = h_t(\lambda \operatorname{Lap}_{h_n}^{P} U^{k+1} + f(U^{k+1})), \quad U^0 = U_0.$$
(11)

Here  $U_0$  denotes the initial condition on mesh grid points. When solving for the numerical solution of (10), one has to sequentially solve a series of nonlinear equations as shown in (11). This is the place in which we should apply the PDHG method. Let us denote the function  $F: \mathbb{R}^{N_x^2} \to \mathbb{R}^{N_x^2}$  as

$$F(U) = U - U^k - h_t(\lambda \operatorname{Lap}_h^P U + f(U)). \tag{12}$$

We want to solve F(U) = 0. As discussed in the introduction, this is equivalent to minimizing  $\iota(F(U))$ , which can further be cast as the following min-max saddle point problem

$$\min_{U \in \mathbb{R}^{N_x^2}} \max_{P \in \mathbb{R}^{N_x^2}} \{L(U, P)\}, \tag{13}$$

where L is defined as  $L(U, P) = P^{\top} F(U)$ . As a result, solving the equation F(U) = 0 finally boils down to the min-max problem (13).

Now the PDHG method suggests the following gradient ascent-descent dynamic for solving (13).

$$P_{n+1} = \underset{P \in \mathbb{R}^{N_X^2}}{\operatorname{argmin}} \left\{ \frac{\|P - P_n\|_2^2}{2\tau_p} - L(U_n, P) \right\} = P_n + \tau_p F(U_n); \tag{14}$$

$$\widetilde{P}_{n+1} = P_{n+1} + \omega(P_{n+1} - P_n);$$
(15)

$$U_{n+1} = \underset{U \in \mathbb{R}^{N_x^2}}{\operatorname{argmin}} \left\{ \frac{\|U - U_n\|_2^2}{2\tau_u} + L(U, \widetilde{P}_{n+1}) \right\} = (\operatorname{Id} + \tau_u \nabla_U F(\cdot)^{\mathsf{T}} \widetilde{P}_{n+1})^{-1} U_n. \tag{16}$$

Similar to our discussion in the introduction, the third line above involves a nonlinear equation that cannot be directly solved. We thus can replace the term  $L(U, \widetilde{P}_{n+1})$  in (16) by the linearization  $\widehat{L}(U, P) = L(U_n, P) + \nabla_U L(U_n, P)(U - U_n)$ , then (16) can be explicitly computed as

$$U_{n+1} = \underset{U \in \mathbb{R}}{\operatorname{argmin}} \left\{ \frac{\|U - U_n\|_2^2}{2\tau_u} + \widehat{L}(U, \widetilde{P}_{n+1}) \right\} = U_n - \tau_u \nabla_U F(U_n)^{\mathsf{T}} \widetilde{P}_{n+1}.$$
(17)

Let us denote  $U_*$  as the solution to F(U) = 0. It is not hard to tell that  $(U_*, 0)$  is a critical point of the functional L(U, P). Furthermore,  $(U_*, 0)$  is the equilibrium point of the time-discrete dynamic (14), (15), (17).

To analyze the convergence speed to the equilibrium state  $(U_*,0)$ , we first consider the affine case in which F(U)=AU-b with A as an  $N_x^2 \times N_x^2$  symmetric matrix. We have the following result, similar to the analysis carried out in [32].

Theorem 1 (Convergence speed in Linear, symmetric case). We fix the extrapolation coefficient  $\omega=2$ . Suppose we obtain the sequence  $\{(U_n,P_n)\}_{n\geq 0}$  by evolving the PDHG dynamic (14), (15), (17) with initial condition  $(U_0,P_0)$ . Suppose F(U)=AU with A symmetric and non-singular. Denote  $\lambda_{\max}$  as the maximum eigenvalue (in absolute value) of A, and denote  $\kappa$  as the condition number of A. Then  $\{(U_n,P_n)\}$  will converge to  $(U_*,0)$  linearly if  $\tau_u\tau_p\leq \frac{4}{3\lambda_{\max}^2}$ . Then the maximum convergence speed is achieved when  $\tau_u\tau_p=\frac{\eta_*}{\lambda_{\max}^2}$ , with the optimal convergence rate  $\gamma_*=\sqrt{1-\frac{\eta_*}{\kappa^2}}$ , i.e., we have for any  $n\geq 1$ ,  $\|(U_n,P_n)-(U_*,0)\|_2\leq \gamma_*^n\|(U_0,P_0)-(U_*,0)\|_2$ . Here  $\eta_*=\eta_*(\kappa)$  is a function of  $\kappa$ . The range of  $\eta_*$  belongs to  $[1,\frac{3}{4})$ .

The proof of the theorem is provided in Appendix A. The explicit form of  $\eta_*(\kappa)$  and  $\gamma_*$  are given in Remark 2 of Appendix A. The optimal convergence rate  $\gamma_*$  will be very close to 1 if the condition number  $\kappa$  is large. Furthermore, one will require  $O(\kappa^2)$  iterations for  $U_n$  to converge. This can be very expensive when A is a large-scale matrix with a large condition number. For example, we consider the heat equation

$$\partial_t u(x,t) = \Delta u(x,t)$$

with periodic boundary conditions. We apply the one-step implicit scheme to this equation, i.e., we consider solving  $(I-\lambda h_t \mathrm{Lap}_{h_x}^\mathrm{P})U^{n+1}=U^n$  at each time step n. Thus  $A=I-h_t\lambda \mathrm{Lap}_{h_x}^\mathrm{P}$ . One can tell that the eigenvalues of A equal  $1+4h_t\lambda N^2\sin^2\left(\frac{\pi k}{N}\right)$  for  $1\leq k\leq N$ . When N is even, the condition number  $\kappa$  of A equals  $1+4\lambda N^2h_t$ . Since we can get rid of the CFL condition by using the implicit scheme, we can pick  $h_t\gg\frac{1}{N^2}$ , which leads to  $\kappa(A)\gg 1$ . The convergence of the primitive PDHG method could be very slow, even for the heat equation.

As discussed in Remark 2,  $\gamma_*$  approaches 0 if the condition number  $\kappa$  drops to 1. Hence, we need to control the condition number of the matrix A to achieve faster convergence speed. This motivates us to introduce the preconditioning technique to the PDHG method. As suggested in both [26] and [32], we replace the  $l^2$  norm used in either  $\|U - U_n\|_2$  or  $\|P - P_n\|_2$  by the G-norm  $\|\cdot\|_G$  which is defined as

$$\|v\|_G = \sqrt{v^\top G v},$$

with G as a symmetric, positive definite matrix. In this work, we mainly focus on substituting the norm  $\|P - P_n\|_2$  with  $\|P - P_n\|_G$ . The PDHG method involving G-norm in its proximal step is sometimes named G-prox PDHG [26]. The dynamic obtained via such G-prox PDHG is shown below.

$$P_{n+1} = P_n + \tau_n G^{-1} F(U_n); \tag{18}$$

$$\widetilde{P}_{n+1} = P_{n+1} + \omega (P_{n+1} - P_n); \tag{19}$$

$$U_{n+1} = U_n - \tau_n \nabla_U F(U_n)^{\top} \widetilde{P}_{n+1}. \tag{20}$$

We should pause here to emphasize to the reader that the above three-line dynamic (18), (19), (20) will be the core gadget for our RD equation solver throughout the remaining part of the paper. Before we move on to further details on solving the RD equation (10) via G-prox PDHG dynamic, let us provide a little more explanation on how (18)-(20) improve the convergence speed  $\gamma_*$ . Analogous to Theorem 1, we have the following corollary for the affine function F.

Corollary 1.1 (Convergence for G-prox dynamic). Suppose we keep all the assumptions in Theorem 1, if we further assume that G commutes with A, i.e., GA = AG, then all the conclusions in Theorem 1 still hold except  $\lambda_{\max}$  now denotes the largest (in absolute value) eigenvalue of  $A^{T}G^{-1}A$ , and  $\kappa^{2}$  now is the condition number of  $A^{T}G^{-1}A$ .

It is now clear that if we can find a matrix G that approximates  $AA^{\top}$  well, then  $A^{\top}G^{-1}A$  will be reasonably close to the identity matrix I. Thus the condition number of  $A^{\top}G^{-1}A$  will hopefully remain close to 1. In such cases, by properly choosing the step size  $\tau_u$ ,  $\tau_p$  such that  $\tau_u\tau_p$  is close to 1, we can obtain a rather fast convergence rate  $\gamma_*$ .

Up to this stage, although most of our intuition and analysis on G-prox PDHG dynamic comes from the case when F is affine, it is natural to extend our treatment to the nonlinear F(U) defined in (12). We may still anticipate the effectiveness of our method since (12) can be recast as

$$F(U) = (I - \lambda h_t \text{Lap}_{h_x}^{\text{P}})U - U^k - h_t f(U),$$

which can be treated as an affine function with a nonlinear perturbation  $h_t f(U)$  carrying the small  $h_t$  coefficient. We now discuss several details in applying the G-prox PDHG dynamic (18)-(20) to the above F(U). We aim at evolving the following dynamic in order to update the implicit one-step scheme (11).

$$P_{n+1} = P_n + \tau_p G^{-1}(U_n - \lambda h_t \text{Lap}_{h_n}^{P} U_n - h_t f(U_n) - U^k);$$
(21)

$$\tilde{P}_{n+1} = P_{n+1} + \omega (P_{n+1} - P_n); \tag{22}$$

$$U_{n+1} = U_n - \tau_u(\widetilde{P}_{n+1} - \lambda h_t \operatorname{Lap}_{h_{\sim}}^{P} \widetilde{P}_{n+1} - h_t f'(U_n) \odot \widetilde{P}_{n+1}). \tag{23}$$

**Initial guess** It is natural to choose the initial value  $U_0$  of the dynamic (21)-(23) as the computed result from the last time step k, i.e., we set  $U_0 = U^k$ ; And we will simply set  $P_0 = 0$ . A more sophisticated choice for  $U_0$  could be the numerical solution at time k + 1 obtained by a forward Euler scheme or an IMEX scheme [38,25].

Choosing the matrix G The function F(U) defined in (12) is dominated by the affine term  $(I - \lambda h_t \operatorname{Lap}_{h_x}^P)^U - U^k$ . It is then natural to choose  $G = (I - \lambda h_t \operatorname{Lap}_{h_x}^P)^2$  as the preconditioner matrix. If the nonlinear term f(U) is a highly stiff term, we may also consider absorbing its Jacobian  $\nabla_U f(U) = \operatorname{diag}(f(U))$  into G. So, G can also be chosen as  $G = (I - \lambda h_t \operatorname{Lap}_{h_x}^P - \operatorname{diag}(f(U)))^2$  in such case. However, there might be a trade-off in doing so: if  $\operatorname{diag}(f(U))$  does not have equal diagonal entries,  $I - \lambda h_t \operatorname{Lap}_{h_x}^P - \operatorname{diag}(f(U))$  cannot be efficiently inverted by Fast Fourier Transform (FFT) or Discrete Cosine Transform (DCT) method. Nevertheless, in most of our experiments, we discover that choosing  $G = (I - \lambda h_t \operatorname{Lap}_{h_x}^P)^2$  is adequate for achieving satisfying convergence speed. For more general reaction-diffusion equations, we discover that the nonlinear function F(U) is usually decomposed as the sum of the linear term AU and the nonlinear term  $h_t f(U)$ . The linear term AU can be treated as the dominating term of F(U). It is then reasonable to choose  $G = AA^T$  or at least close to  $AA^T$  as a decent preconditioner of our method. This strategy works properly on general RD equations such as the Cahn-Hilliard equation or higher-order equations arising in polymer science. We refer the reader to examples in section 4 for details.

**Application of FFT for fast computation** Making use of the Fast Fourier Transform (FFT) method, or more precisely, 2-dimensional FFT [23] to accelerate our computation is crucial in our method. There are two places where we should apply FFT. The first is where we compute  $G^{-1}u$ ; the second is where we compute  $Lap_{h_x}^Pu$ . We refer the readers to chapter 4.8 of [23] and the references therein for details on implementing FFT. We also refer the reader to the examples in section 4 for applying FFT to general RD equations.

**Choose suitable stepsize** For the affine case discussed in Corollary 1.1, if G is close to  $AA^{\mathsf{T}}$ , then  $\lambda_{\max}(A^{\mathsf{T}}G^{-1}A)$  should be a close to 1, then  $\tau_u\tau_p \leq \frac{4}{3\lambda_{\max}^2}$  indicates that we could choose stepsizes  $\tau_u,\tau_p$  rather large. In our practice, starting at  $\tau_u=\tau_p=0.8$  should be a reasonable choice. One can increase or decrease the stepsize based on the actual performance of the method.

**Stopping criterion** During our computation, we will set up a threshold  $\delta$  for our method. After each iteration of the PDHG dynamic, we evaluate the  $l^2$  norm of the residual  $\operatorname{Res}(U_n) = \frac{U_n - U^k}{h_l} - (\lambda \operatorname{Lap}_{h_x}^P U_n + f(U_n))$ , we terminate the PDHG iteration iff  $\|\operatorname{Res}(U_n)\|_2 \le \delta$ .

Remark 1 (Neumann boundary condition and DCT). It is worth providing some further discussions on our treatment of the Neumann boundary condition (BC), i.e., for a particular rectangular region  $\Omega \subset \mathbb{R}^2$ ,  $\frac{\partial u}{\partial \tilde{n}} = 0$  on  $\partial \Omega$ . We discretize both sides of  $\Omega$  into  $N_x - 1$  subintervals. Thus the space stepsize  $h_x = \frac{L}{N_x - 1}$ . Such discretization will lead to  $N_x^2$  mesh grid points. For point  $(ih_x, 0)$  on the vertical boundary of  $\Omega$ , we apply the central difference scheme to the Neumann boundary condition at the midpoint  $(ih_x, -\frac{1}{2}h_x)$ , which leads to  $\frac{U_{i,-1}-U_{i,0}}{h_x} = 0$ , thus  $U_{i,-1} = U_{i,0}$ . Similar treatments are applied to the other boundaries of  $\Omega$ . Suppose we consider

using the central difference scheme to discretize the Laplacian  $\Delta$ , let us denote the discretized Laplacian w.r.t. Neumann boundary condition as  $\text{Lap}_{h_{\omega}}^{N}$ , then  $\text{Lap}_{h_{\omega}}^{N}$  takes the following form.

$$\operatorname{Lap}_{h_{x}}^{N} = \frac{1}{h_{x}^{2}} \begin{bmatrix} L_{1} & I & & & & \\ I & L_{2} & I & & & & \\ & \ddots & \ddots & \ddots & & \\ & & I & L_{2} & I & & \\ & & & I & L_{1} \end{bmatrix}_{N_{x} \times N_{x} \text{blocks}} . \tag{24}$$

Here the block matrices  $L_1, L_2$  are

$$L_1 = \begin{bmatrix} -2 & 1 & & & & \\ 1 & -3 & 1 & & & \\ & \ddots & \ddots & \ddots & \\ & & 1 & -3 & 1 \\ & & & 1 & -2 \end{bmatrix}_{N_x \times N_x}, \quad L_2 = \begin{bmatrix} -3 & 1 & & & \\ 1 & -4 & 1 & & \\ & \ddots & \ddots & \ddots & \\ & & 1 & -4 & 1 \\ & & & 1 & -3 \end{bmatrix}_{N_x \times N_x}$$

Similar to using FFT for the computation involving  $\operatorname{Lap}_{h_x}^P$ , we can use the Discrete Cosine Transform (DCT) [48] [23] to efficiently evaluate matrix-vector multiplication or solve linear equations involving the matrix  $\operatorname{Lap}_{h_x}^N$ . To be more specific, we use the DCT-2 transform introduced in [48] in the 2-dimensional scenario which enjoys the  $O(N_x^2 \log N_x)$  computational complexity.

We summarize our method in the following algorithm. It is not hard to tell that the total complexity of each inner PDHG method is  $O(\sharp \{\text{PDHG iter}\} \cdot N_x^2 \log N_x\})$ .

## Algorithm 1 PDHG method for updating implicit one-step FD scheme of RD equation.

```
1: Input: Initial condition u_0, terminal time T, number of time subintervals N,; region size L, number of space subintervals N,;
 2: Initialize h_t = T/N_t, h_x = L/N_x, \{U_{ij}^0\} = \{u_0(ih_x, jh_x)\}.
 3: for 0 \le k \le N_t - 1 do
         Set initial condition: U_0 = U^k (or \hat{U}^{k+1} obtained via explicit Euler or IMEX scheme).
 5:
 6:
         while \|\operatorname{Res}(U_n)\|_2 \ge \delta do
             Evolve the G-prox PDHG dynamic (21)-(23) with help of 2D FFT(DCT):
 7.
 8:
              We use FFT for periodic BC and DCT for Neumann BC.
              Compute V_n = \text{Lap}_{h_n}^{P} U_n via 2D FFT(DCT);
 9:
             Compute W_n = U_n - \lambda h_t V_n - h_t f(U_n) - U^k;
10.
              Solve GY_n = W_n via 2D FFT(DCT);
11:
             Update P_{n+1} = P_n + \tau_p Y_n; \widetilde{P}_{n+1} = P_{n+1} + \omega (P_{n+1} - P_n);
12:
13:
             Compute Q_{n+1} = \text{Lap}_{h}^{P} \widetilde{P}_{n+1} via 2D FFT(DCT);
14:
             Update U_{n+1} = U_n - \tau_u(\widetilde{P}_{n+1} - \lambda h_t Q_{n+1} - h_t f'(U_n) \odot \widetilde{P}_{n+1});
15:
             n = n + 1:
16:
         end while
17:
         Set U^{k+1} = U_{..};
18: end for
19: Output: The numerical solution U^0, U^1, ..., U^{N_t}.
```

In this section, we mainly focus on the one-step implicit finite difference (FD) scheme to illustrate how we apply the PDHG iterations to update the given FD scheme. But we should emphasize that our method is not restricted to such a scheme. One can extend the PDHG method to various types of numerical schemes by formulating the scheme at a certain time step k as a nonlinear equation  $F^k(U) = 0$ , and construct the functional  $L^k(U, P) = P^T F^k(U)$ . Then one can apply the dynamic (18)-(20) to update the numerical solution from  $U^k$  to  $U^{k+1}$ . In addition, our method is applicable to more general reaction-diffusion equations (systems). Further discussions and details are supplied in section 4.

#### 3.2. Discussion on convergence criteria and adaptive $h_t$ method

Theorem 1 suggests that under the linear case, the convergence of PDHG method relies on condition number  $\kappa$ , which is directly related to  $h_x$ ,  $h_t$  of our discrete scheme. In practice, we fix  $h_x$  and  $\tau_u$ ,  $\tau_p$  in the algorithm. At every time step n we discover that when time stepsize  $h_t$  gets larger than a certain threshold value  $h_t^*$  which depends on  $h_x$ ,  $\tau_u$ ,  $\tau_p$  and n, PDHG method will hardly converge. The method works well when  $h_t$  is slightly smaller than the threshold. The theoretical study on how  $h_t^*$  guarantees the convergence of our method will be an important future research direction.

**Adaptive time stepsize** As discussed above, we cannot guarantee the convergence of the PDHG iteration (21)-(23) for any time stepsize  $h_t$ . Since the aforementioned threshold  $h_t^*$  may vary at different time stages, and how  $h_t^*$  varies depends on the nature of the equation as well as the discretization scheme. Given the potential difficulty of choosing the suitable  $h_t$  that guarantees both the

numerical accuracy as well as the convergence of the PDHG iterations, we come up with the strategy of using adaptive stepsize  $h_t$ throughout the computation. We choose a time stepsize  $h_i^0$  that guarantees the numerical accuracy and will serve as the upper bound of all  $h_t$  throughout our method, we also set up two integers  $N^* > N_* > 0$  as the thresholding integers for enlarging or shrinking the time stepsize  $h_t$ . We also pick a rescaling coefficient  $\eta \in (0,1)$ . During each time step n of the algorithm, we record the total number of PDHG iterations  $M_{\rm PDHG}$ , and reset the stepsize  $h_t$  for the next time step based on the following rules:

- If  $M_{\rm PDHG} > N^*$ , we shrink  $h_t$  by rate  $\eta$ ,  $h_t = \eta h_t$ ;
- If  $N^* \geq M_{\mathrm{PDHG}} \geq N_*$ , we remain  $h_t$  unchanged; If  $M_{\mathrm{PDHG}} < N_*$ , we enlarge  $h_t$  by rate  $\frac{1}{\eta}$ ,  $h_t = \frac{h_t}{\eta}$ , if  $\frac{h_t}{\eta} \leq h_t^0$ ; we remain  $h_t$  unchanged if  $\frac{h_t}{\eta} > h_t^0$ .

It is also reasonable to fix  $h_x, h_t$  but to only shrink the PDHG stepsizes  $\tau_u, \tau_p$  when we encounter difficulties in converging. However, according to our experience, shrinking  $\tau_u$ ,  $\tau_p$  usually requires much more PDHG iterations for convergence, which may cause the algorithm less efficient compared with the aforementioned adaptive  $h_t$  strategy.

#### 4. Numerical examples

In this section, we demonstrate some numerical results computed by the proposed method. Throughout our experiments, we always use the extrapolation coefficient  $\omega = 1$ , and set the initial condition  $U_0$  as the numerical solution  $U^k$  computed from the last time step  $t_k$ . One can also try other values of  $\omega$  or a more sophisticated initial guess of  $U_0$ . Our experiences show that confining  $\omega$ around 1 will probably provide the best performance of the PDHG method. Choosing  $U_0$  as  $\hat{U}^{k+1}$  obtained by a specific explicit or IMEX scheme may slightly shorten the convergence time of the PDHG iteration. However, it is worth mentioning that when we are dealing with stiff equations, such treatment may introduce instability to the PDHG dynamic which may lead to the blow-up of the method.

Furthermore, as we have emphasized before, the mission of this paper is to verify the correctness and effectiveness of the proposed PDHG method in resolving the equation F(U) = 0 at each time step. Thus, in this work, we will mainly focus on the straightforward one-step implicit scheme (11) in all numerical examples by omitting further discussions and experiments on more sophisticated numerical schemes.

We use fixed time stepsize  $h_t$  in our numerical examples unless we emphasize that the adaptive  $h_t$  method is applied in the

Our numerical examples are computed in MATLAB on a laptop with 11th Gen Intel(R) Core(TM) i5-1135G7 @ 2.40 GHz 2.42 GHz CPU.

#### 4.1. Allen-Cahn equations

The Allen-Cahn equation [1] is a typical reaction-diffusion equation taking the following form

$$\frac{\partial u(x,t)}{\partial t} = a\Delta u(x,t) - bW'(u(x,t)), \text{ on } \Omega \subset \mathbb{R}^2, \quad u(\cdot,0) = u_0.$$
 (25)

Here a, b > 0 are positive coefficients,

$$W(u) = \frac{(u^2 - 1)^2}{4} \tag{26}$$

is a double-well potential function with its derivative  $W'(u) = u^3 - u$ . We will always assume periodic boundary conditions in our

The Allen-Cahn equation can be treated as the  $L^2$ -gradient flow of the following functional  $\mathcal{E}(u)$ .

$$\mathcal{E}(u) = \int_{\Omega} \frac{1}{2} a |\nabla u|^2 + bW(u) \, dx. \tag{27}$$

### 4.1.1. Examples with shrinking level set curve

In the first example, we consider  $\Omega = [-L, L]^2$  with L = 0.25. We consider taking  $a = \epsilon$ ,  $b = \frac{1}{\epsilon}$  with  $\epsilon = 0.01$ . Let use consider  $u_0 = 2\chi_B - 1$ . Here  $\chi_E$  denotes the indicator function of measurable set E, i.e.,  $\chi_E(x) = 1$  if  $x \in E$ , and  $\chi_E(x) = 0$  otherwise. We denote B as the disk centered at O with a radius equal to 0.2. Suppose we use periodic boundary conditions for (25). It is well-known that the zero-level-set curve of the solution u(x,t) to Allen-Cahn equation behaves similarly to the mean curvature flow as time t increases [40,35,34]. In this case, we can treat the initial level set curve as the circle centered at the origin with radius r(0) = 0.2. As t increases, the circle radius will shrink at the rate of  $\epsilon$  times circle curvature, i.e.,  $\dot{r}(t) = -\epsilon \kappa(t) = -\frac{\epsilon}{r(t)}$ . Solving this equation leads

to  $r(t) = \sqrt{r(0)^2 - 2\epsilon t}$ . Thus the level set circle will vanish at finite time  $t = \frac{r(0)^2}{2\epsilon} = 2$ . As suggested in section 4.4 of [35], it is important to choose the spatial stepsize  $h_x$  small enough so that  $h_x$  no larger than  $O(\epsilon)$  to capture the shrinkage of level set curve, otherwise, the numerical solution may get stuck at some intermediate stage. In this example, we solve the equation on time interval [0,3]. We choose  $N_t = 3000$ , thus  $h_t = 1/1000$ ;  $N_x = 100$  with  $h_x = L/N_x = 1/200$ . Recall

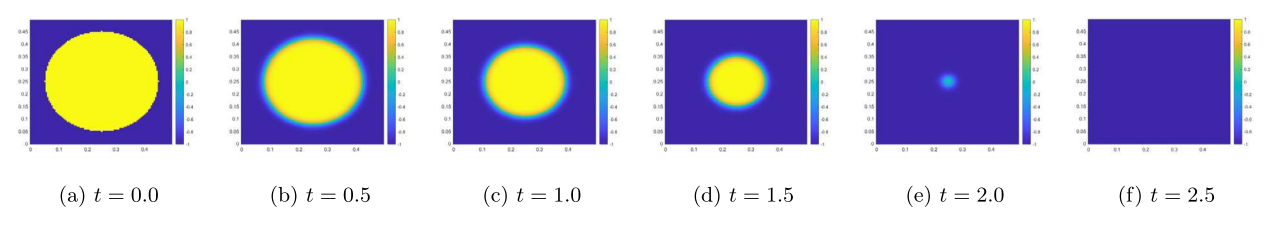


**Fig. 1.** Numerical solution of (1) at different times with initial condition  $u_0 = 2\chi_B - 1$ . (For interpretation of the colors in the figure(s), the reader is referred to the web version of this article.)

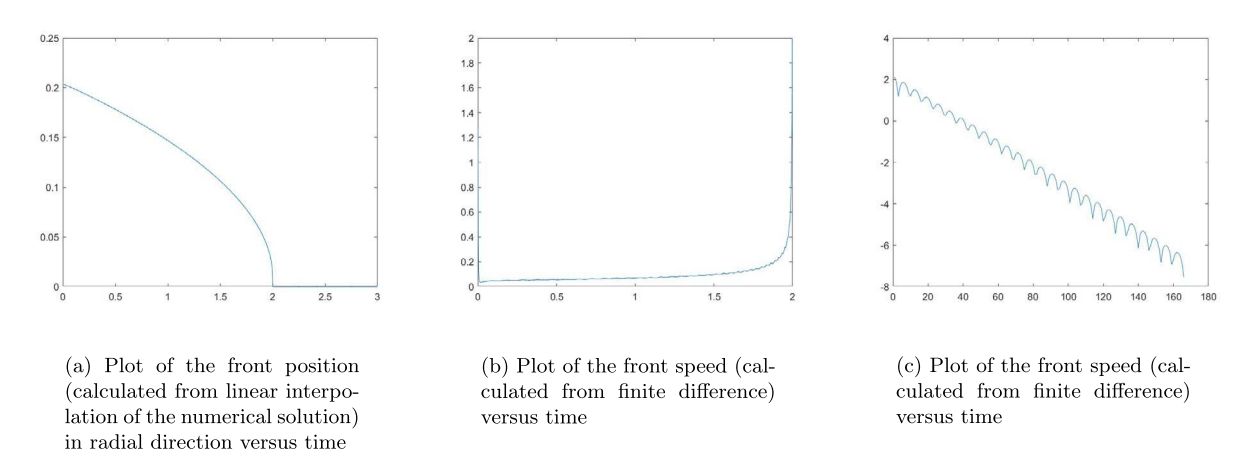


Fig. 2. Plots of front position and speed (Left & Middle); Plots of  $\log_{10} \operatorname{Res}(U_n)$  versus PDHG iterations at time stage t = 1.0 (Right).

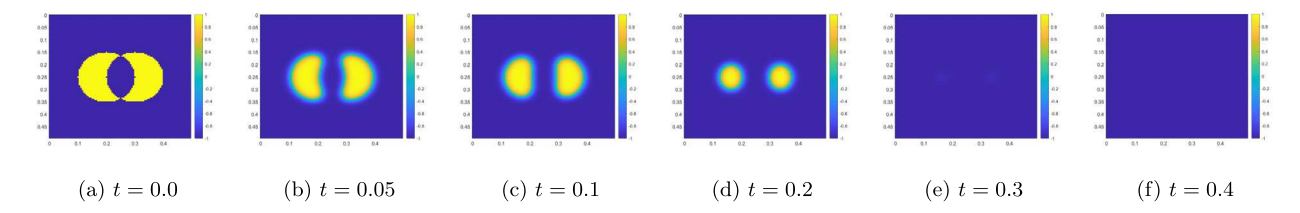


Fig. 3. Numerical solution at different times with initial condition  $u_0 = 2\chi_E - 1$ . Notice that in the last plot, we have almost converged to the equilibrium solution u = -1.

 $h_x < \varepsilon$ . We choose  $\tau_u = \tau_p = 0.5$  as the stepsize for the PDHG iteration. Some computed results are shown in Fig. 1. Plots of the radial position as well as the moving speed of the front (zero level set circle) of the numerical solution are presented in Fig. 2.

We apply the PDHG method described in Algorithm 1 to this problem. Although equation (1) contains a nonlinear term with a significant coefficient  $\frac{1}{\epsilon}$ , our proposed PDHG method still solves the nonlinear F(U)=0 efficiently. To be more specific, we set the PDHG-threshold  $\delta=10^{-7}$ . Most PDHG iterations will terminate in less than 200 steps for each discrete time step. The right plot of Fig. 2 indicates the linear convergence of the proposed method.

We also solve equation (1) on  $\Omega = [0,0.5]^2$  within the time interval [0,0.5]. We still set  $a = \epsilon, b = \frac{1}{\epsilon}$  with  $\epsilon = 0.01$ . We pick  $N_x = 100$ ,  $N_t = 500$ , thus  $h_x = 1/200$ ,  $h_t = 1/1000$ . We consider the initial condition  $u_0 = 2\chi_E - 1$  with the region  $E = (B_1 \setminus B_2) \cup (B_2 \setminus B_1)$ , where  $B_1, B_2$  are disks centered at (0.2, 0.25), (0.3, 0.25) with radius both equal to 0.1. We apply the PDHG method with  $\tau_u = \tau_p = 0.5$  and obtain the numerical results in Fig. 3. In this example, the PDHG method takes no more than 200 iterations for each time step update.

#### 4.2. Cahn-Hilliard equations

We now switch to another well-known reaction-diffusion equation known as the Cahn-Hilliard equation [5], which takes the following form.

$$\frac{\partial u(x,t)}{\partial t} = -a\Delta\Delta u(x,t) + b\Delta W'(u(x,t)), \text{ on } \Omega \subset \mathbb{R}^2, \quad u(\cdot,0) = u_0.$$
 (28)

Here we assume a, b > 0, and W(u) defined the same as in the Allen-Cahn equation. In this section, we will restrict our discussion to periodic boundary conditions. Similar to the Allen-Cahn equation, the Cahn-Hilliard equation can be treated as the  $H^{-1}$ -gradient flow of the functional  $\mathcal{E}(u)$  defined in (27). For this reason, compared with the Allen-Cahn equation, the Cahn-Hilliard equation

Table 1

Data / Circles.							
	1		3		5	6	7
$x_i$	$\pi/2$	$\pi/4$ $3\pi/4$ $2\pi/15$	$\pi/2$	$\pi$	$3\pi/2$	π	$3\pi/2$
$y_i$	$\pi/2$	$3\pi/4$	$5\pi/4$	$\pi/4$	$\pi/4$	$\pi$	$3\pi/2$
$r_i$	$\pi/5$	$2\pi/15$	$\pi/15$	$\pi/10$	$\pi/10$	$\pi/4$	$\pi/4$

involves one extra operator  $-\Delta$  on the right-hand side of the equation. This difference leads to several slight modifications to our original algorithm.

The functional F(U) introduced in (12) is now

$$F(U) = (I - \lambda h_t \operatorname{Lap}_h^{P} \operatorname{Lap}_h^{P}) U - U^k - h_t \operatorname{Lap}_h^{P} f(U).$$
(29)

Thus  $L(U,P) = P^{\top}((I - \lambda h_t \operatorname{Lap}_{h_x}^{\operatorname{P}} \operatorname{Lap}_{h_x}^{\operatorname{P}})U - U^k) - h_t P^{\top} \operatorname{Lap}_{h_x}^{\operatorname{P}} f(U)$ . It is then natural to choose precondition matrix G as  $(I - \lambda h_t \operatorname{Lap}_h^{\operatorname{P}} \operatorname{Lap}_h^{\operatorname{P}})^2$ . The three-step PDHG update for Cahn-Hilliard equation can thus be formulated as

$$P_{n+1} = P_n + \tau_p G^{-1}(U_n - \lambda h_t \text{Lap}_{h_v}^{P} \text{Lap}_{h_v}^{P} U_n - h_t \text{Lap}_{h_v}^{P} f(U_n) - U^k);$$
(30)

$$\widetilde{P}_{n+1} = P_{n+1} + \omega (P_{n+1} - P_n); \tag{31}$$

$$U_{n+1} = U_n - \tau_u(\widetilde{P}_{n+1} - \lambda h_t \operatorname{Lap}_{h_x}^{\operatorname{P}} \operatorname{Lap}_{h_x}^{\operatorname{P}} \widetilde{P}_{n+1} - h_t f'(U_n) \odot \operatorname{Lap}_{h_x}^{\operatorname{P}} \widetilde{P}_{n+1}). \tag{32}$$

By carefully investigating the steps among (30)-(32), one can tell that both the linear equation involving G and the matrix-vector multiplication involving  $\operatorname{Lap}_{h_x}^P$  can be computed via FFT, which indicates the effectiveness of the computational scheme when applied to Cahn-Hilliard equations.

We demonstrate several numerical examples below.

#### 4.2.1. Example with seven circles

Inspired by the second example introduced in [14], we consider Cahn-Hilliard equation (28) on periodic domain  $\Omega = [0, 2\pi]^2$  with  $a = 0.1^2$  and b = 1. We set the initial condition  $u_0$  as

$$u_0(x, y) = -1 + \sum_{i=1}^{7} \varphi(\sqrt{(x - x_i)^2 + (y - y_i)^2} - r_i),$$

where the mollifier function  $\varphi$  is defined as

$$\varphi(s) = \begin{cases} 2e^{-\frac{\epsilon^2}{s^2}} & s < 0; \\ 0 & s \ge 0 \end{cases}, \text{ with } \epsilon = 0.1.$$

One can treat  $u_0(x, y)$  as an indicator function where its value is equal to +1 if (x, y) falls inside any of the seven circles and is equal to -1 otherwise. Furthermore, we define the centers and radii of these seven circles as listed in Table 1.

We will solve equation (28) on the time interval [0,30]. In our numerical implementation, we set  $N_x=128$ ,  $h_x=\pi/64$ ;  $N_t=6000$ ,  $h_t=1/200$ . For the PDHG iteration, we set  $\tau_u=\tau_p=0.5$ . The numerical solution to this equation is demonstrated in Fig. 4. The plots of log residuals at different time stages are also presented in Fig. 4, which exhibit the linear convergence of the PDHG algorithm. The small circles will gradually fade out, leaving the largest circle in the center of the domain till the end. By analyzing our numerical solution, the time  $T_1$  at which the value of our numerical solution is evaluated at  $(\pi/2,\pi/2)$  passes 0 is located in the interval [6.340,6.345]; while the time  $T_2$  at which our numerical value evaluated at  $(3\pi/2,3\pi/2)$  passes 0 is located in the interval [26.015,26.020]. Both times meet the accuracy proposed in [14].

#### 4.2.2. Example with sinusoidal initial condition

In this section, we follow example 4 proposed in [14] to compute (28) on  $\Omega = [0, 2\pi]^2$ . We set  $a = \frac{\pi^2}{25000}$ , b = 1. The initial condition is set as

$$u_0(x, y) = 0.05(\cos(3x)\cos(4y) + (\cos(4x)\cos(3y))^2 + \cos(x - 5y)\cos(2x - y)).$$

We solve the equation on the time interval [0,8]. We set  $N_x = 256$ ,  $h_x = \pi/128$ ;  $N_t = 24000$ ,  $h_t = 1/3000$ . For the PDHG part, we choose  $\tau_u = \tau_p = 0.5$ . The PDHG iteration is working efficiently at every time stepsize. Some numerical plots are shown in Fig. 5.

#### 4.2.3. Example with random initial condition

One can also consider the Cahn-Hilliard equation (28) with random initial condition. This may impose more challenges to our computation since the randomness will remove the regularity of  $u_0$  and make the numerical computation unstable. We will solve the equation (28) on [0,1] in this example. We let the periodic domain  $\Omega = [0,1]^2$ . Then we choose  $N_x = 128$ ,  $h_x = 1/128$ ;  $N_t = 100000$ 

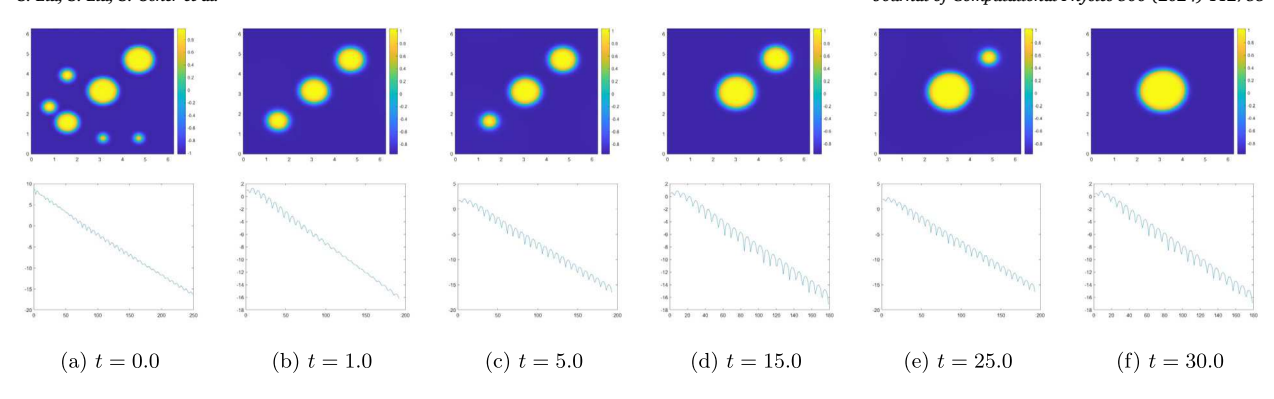


Fig. 4. Numerical solution and  $\log_{10} \operatorname{Res}(U_n)$  plot at different time stages for the seven circle example. The residual plots indicate the linear convergence of PDHG method for the nonlinear objective functions used in this example.

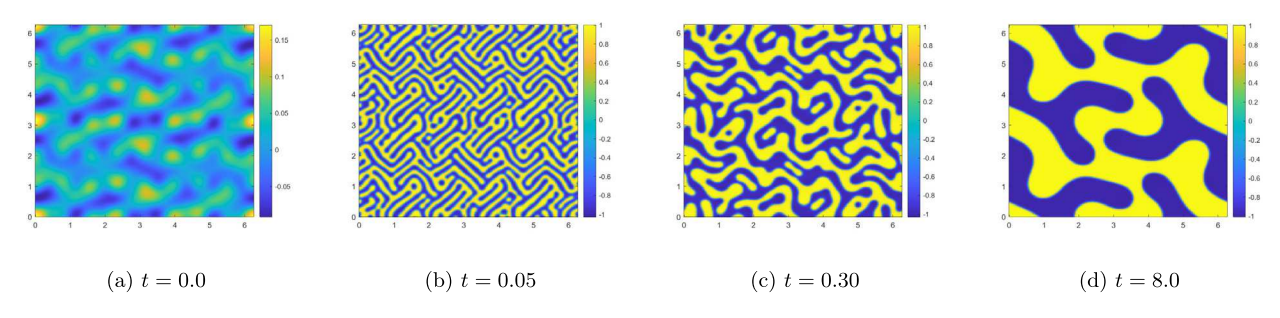


Fig. 5. Numerical solution at different time stages with sinusoidal initial condition.

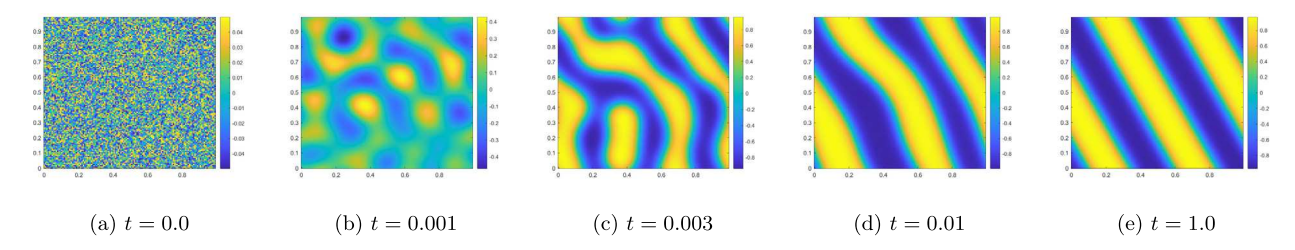


Fig. 6. Numerical solution at different time stages with random initial condition.

with  $h_t = 1/100000$ . We choose a rather small time step size in this example in order to guarantee the accuracy of our numerical solution. For the initial condition, we choose  $u_0$  as a random scalar field that takes i.i.d. values uniformly distributed on [-0.05, 0.05]. We evolve the PDHG dynamic with stepsize  $\tau_u = \tau_p = 0.75$ . We plot the numerical solutions at certain time stages in Fig. 6. The reaction-diffusion system reaches the equilibrium state at t = 1. The residual plots of Res(U) at time t = 0.01 and t = 1 are provided in Fig. 7.

#### 4.3. Higher-order reaction-diffusion equations

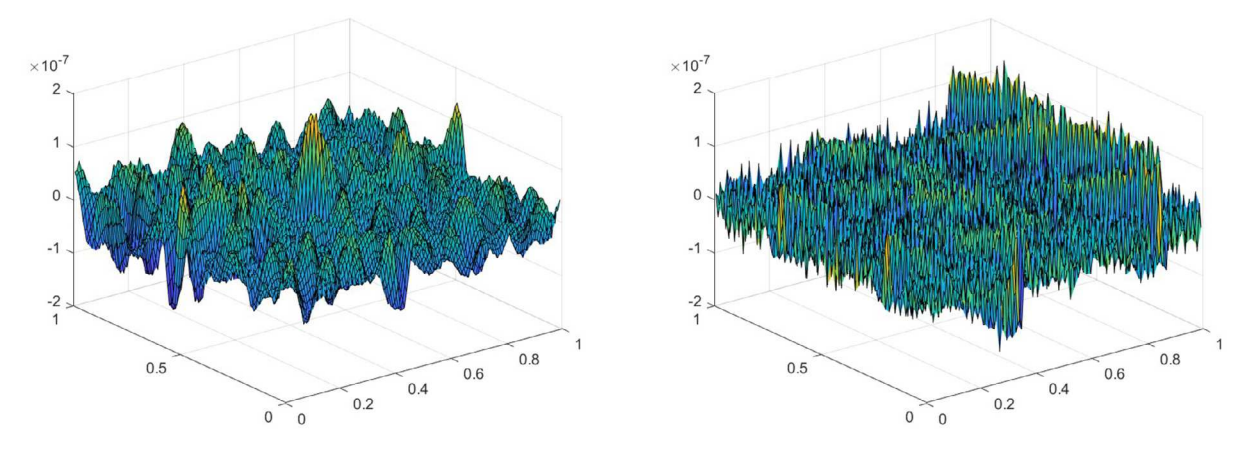
In addition to the Allen-Cahn and Cahn-Hilliard equations, we test the method on the following 6th-order Cahn-Hilliard-type equation.

$$\frac{\partial u(x,t)}{\partial t} = \Delta(\epsilon^2 \Delta - W''(u) + \epsilon^2)(\epsilon^2 \Delta u - W'(u)) \text{ on } \Omega, \quad u(\cdot,0) = u_0.$$
(33)

The above equation was first proposed in [22] which depicts the pore formation in functionalized polymers. This equation was later studied in the numerical examples of [13]. In this example, we set  $\Omega = [0, 2\pi]^2$ . We choose parameter  $\epsilon = 0.18$ . The potential function W(u) is the same as defined in (26). Thus  $W'(u) = u^3 - u$ ,  $W''(u) = 3u^2 - 1$ . Similar to Allen-Cahn or Cahn-Hilliard equations, equation (33) can also be treated as a flow that dissipates the energy  $\mathcal{E}(u)$  with  $a = \epsilon^2$ , b = 1.

In our numerical implementation of the PDHG method, the functional F(U) is now

$$F(U) = U - h_t \operatorname{Lap}_{h_-}^{P}(\epsilon^2 \operatorname{Lap}_{h_-}^{P} - \operatorname{diag}(W''(U)) + \epsilon^2 I)(\epsilon^2 \operatorname{Lap}_{h_-}^{P} U - W'(U)) - U^k.$$



(a) Plot of the residual Res(U) at t = 0.01

(b) Plot of the residual Res(U) at t = 1.0

**Fig. 7.** Plots of residual at t = 0.01 and t = 1.0.

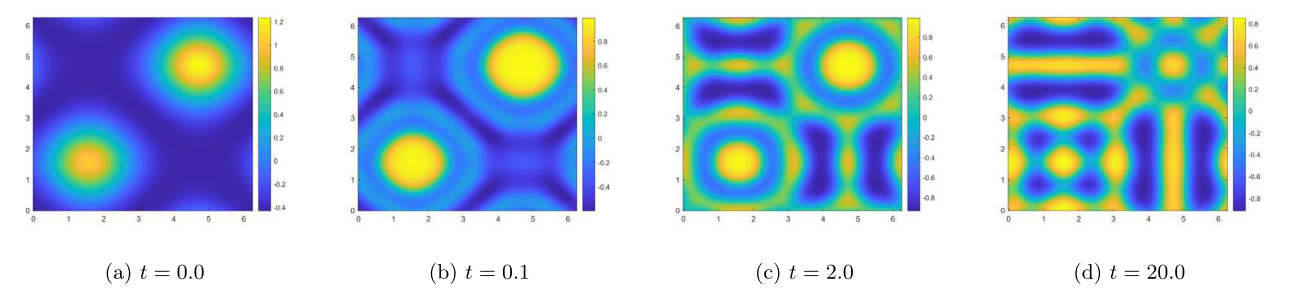


Fig. 8. Numerical solution at different time stages with initial condition (34).

Similar to Allen-Cahn and Cahn-Hilliard equations, we pick the preconditioner G as the square of the matrix in the dominating linear part of F(U). However, if we directly keep the diagonal matrix  $\operatorname{diag}(W''(U))$ , we will not be able to invert G efficiently by using FFT. Since the value of W''(u) close to the equilibrium states  $\pm 1$  is approximately 2, we follow a similar idea in [13] to replace such matrix with 2I. Thus, in this problem, we set  $G = (I - h_I \epsilon^2 \operatorname{Lap}_{h_X}^P - (2 - \epsilon^2)I)\operatorname{Lap}_{h_X}^P)^2$  which can be inverted via FFT algorithm. Now the 3-line PDHG update is formulated as

$$\begin{split} P_{n+1} &= P_n + \tau_p G^{-1}(U_n - h_t \mathrm{Lap}_{h_x}^{\mathrm{P}} \widetilde{\mathrm{Lap}}_{h_x}(\epsilon, U_n))(\epsilon^2 \mathrm{Lap}_{h_x}^{\mathrm{P}} U_n - W'(U_n)) - U^k); \\ \widetilde{P}_{n+1} &= P_{n+1} + \omega(P_{n+1} - P_n); \\ U_{n+1} &= U_n - \tau_u (\widetilde{P}_{n+1} - h_t(\epsilon^2 \mathrm{Lap}_{h_x}^{\mathrm{P}} - \mathrm{diag}(W''(U))) \widetilde{\mathrm{Lap}}_{h_x}(\epsilon, U_n) \mathrm{Lap}_{h_x}^{\mathrm{P}} \widetilde{P}_{n+1} \\ &\quad + h_t(\epsilon^2 \mathrm{Lap}_{h_x}^{\mathrm{P}} U_n - W'(U_n)) \odot W'''(U_n) \odot \mathrm{Lap}_{h_x}^{\mathrm{P}} \widetilde{P}_{n+1}). \end{split}$$

Here we denote  $\widetilde{\operatorname{Lap}}_{h_x}(\epsilon,U) = \epsilon^2 \operatorname{Lap}_{h_x}^P - \operatorname{diag}(W''(U)) + \epsilon^2 I$ . If the size of U is  $N_x^2$ , one can verify that all calculations among the PDHG iteration can be computed with complexity  $O(N_x^2 \log(N_x))$  via the FFT method.

Similar to [13], we choose initial condition

$$u_0(x, y) = 2e^{\sin x + \sin y - 2} + 2.2e^{-\sin x - \sin y - 2} - 1.$$
 (34)

In the numerical implementation, we solve the equation (33) from t=0 to t=20. We choose  $N_x=128$ ,  $N_t=\pi/64$ ;  $N_t=20000$ ,  $N_t=1/1000$ . We choose the PDHG stepsizes  $\tau_u=\tau_p=0.58$ . We choose the threshold for terminating the iteration as  $\delta=0.5\times 10^{-5}$ . We present some of the results in Fig. 8 and Fig. 9.

#### 4.4. Reaction-diffusion systems

We have already shown some reaction-diffusion equation examples in the previous sections. We now apply the method to compute reaction-diffusion systems.

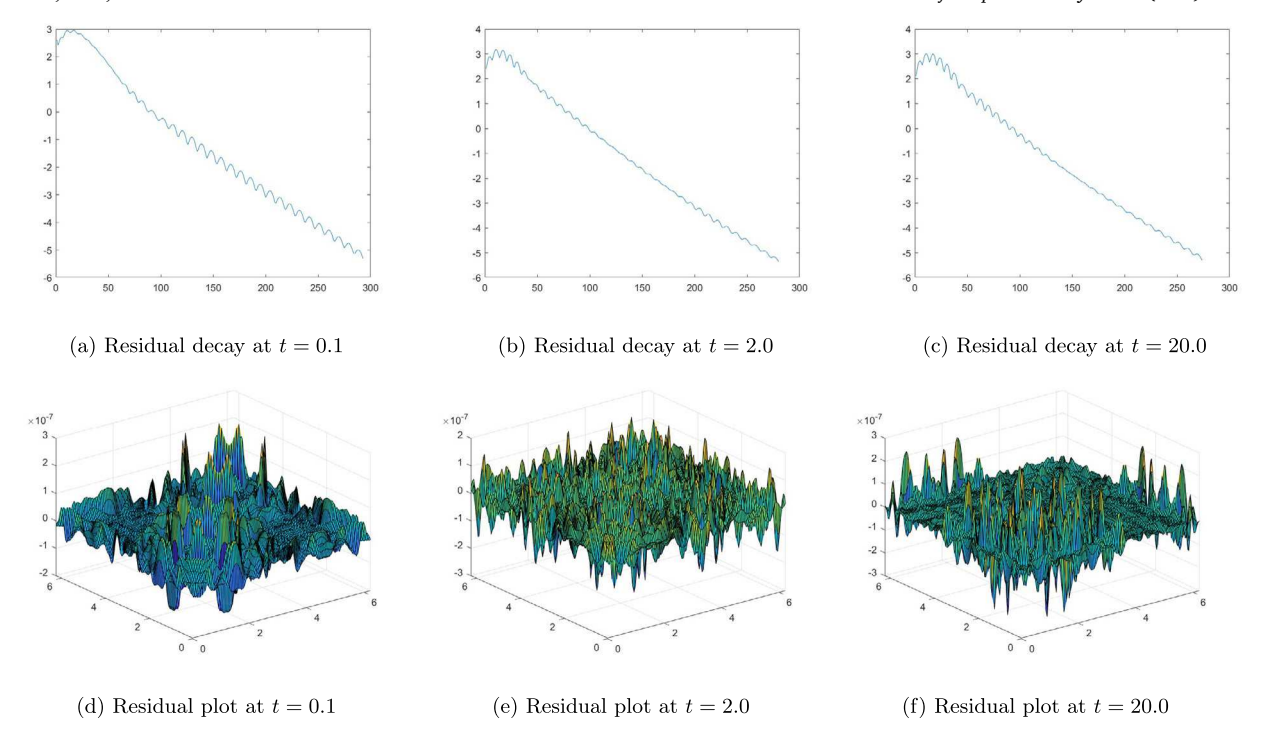


Fig. 9. The log-residual decay & plots of residual functional  $Res(U^n)$  at different time stages t = 0.1, 2.0, 20.0.

#### 4.4.1. Schnakenberg model

The Schnakenberg model is first considered in [41] to model the limit-cycle behavior in a two-component chemical reaction system. In the discussion, we consider the following reaction-diffusion PDE system defined on unit square  $\Omega = [0, 1]^2$  where u, v represent the density concentration of two chemicals. Such a PDE system is also investigated in references [25,53].

$$\frac{\partial u(x, y, t)}{\partial t} = D_1 \Delta u(x, y, t) + \kappa (a - u + u^2 v),\tag{35}$$

$$\frac{\partial v(x, y, t)}{\partial t} = D_2 \Delta v(x, y, t) + \kappa (b - u^2 v). \tag{36}$$

The initial condition of the system is

$$u(x, y, 0) = a + b + 10^{-3} * e^{-100((x - \frac{1}{3})^2 + (y - \frac{1}{2})^2)}, \quad v(x, y, 0) = \frac{b}{(a + b)^2}.$$
 (37)

Here we set  $\kappa = 100$ , a = 0.1305, b = 0.7695,  $D_1 = 0.05$ ,  $D_2 = 1$ . One can understand the initial data as exerting a tiny perturbation to the equilibrium solution  $(a + b, \frac{b}{(a+b)^2})$  of the Schnakenberg system (35), (36). Such an equilibrium state is unstable, the small perturbation will lead to the formation of certain dotted patterns in both components u and v.

perturbation will lead to the formation of certain dotted patterns in both components u and v.

We assume the Neumann boundary condition  $\frac{\partial u}{\partial n} = 0$  on  $\partial \Omega$  where  $\frac{\partial}{\partial n}$  denotes the directional derivative w.r.t. the outer pointing normal direction  $\boldsymbol{n}$ .

Suppose we apply the one-step implicit scheme to solve this problem, recall the discrete Laplacian with Neumann BC introduced in (24), at the k-th time step, we consider

$$\begin{split} F_u(U,V) &= U - U^k - h_t(D_1 \mathrm{Lap}_{h_x}^\mathrm{N} U + \kappa (a\mathbf{1} - U + U^2 \odot V)); \\ F_v(U,V) &= V - V^k - h_t(D_2 \mathrm{Lap}_{h_x}^\mathrm{N} V + \kappa (b\mathbf{1} - U^2 \odot V)). \end{split}$$

At each time step, our purpose is to solve  $F_u(U,V)=0$ ,  $F_v(U,V)=0$  for updating  $U^k,V^k$ . By treating  $\widetilde{U}=(U,V)\in\mathbb{R}^{2N_x^2}$  as an entity; and by denoting  $\widetilde{F}:\mathbb{R}^{2N_x^2}\to\mathbb{R}^{2N_x^2},\widetilde{U}\mapsto (F_u(U,V)^\top,F_v(U,V)^\top)^\top$ , the problem of solving  $\widetilde{F}(\widetilde{U})=0$  reduces to the scenario of solving single F(U)=0 discussed before. Hence, it is natural to introduce the dual variable  $\widetilde{P}=(P,Q)\in\mathbb{R}^{2N_x^2}$ ; The stiff Laplacian terms can be treated as dominating linear terms of both functions F,G, thus we set our preconditioner matrix  $\widetilde{G}=\begin{pmatrix}G_u\\G_v\end{pmatrix}$  with  $G_u=(I-h_tD_1\mathrm{Lap}_{h_x}^\mathrm{N})^2$  and  $G_v=(I-h_tD_2\mathrm{Lap}_{h_x}^\mathrm{N})^2$ . The corresponding PDHG iteration for solving  $\widetilde{F}(\widetilde{U})=0$  is formulated as follows.

$$P_{n+1} = P_n + \tau_p G_u^{-1}(U_n - U^k - h_t(D_1 \text{Lap}_{h_{-}}^N U_n + \kappa(a\mathbf{1} - U_n + U_n^2 \odot V_n)));$$

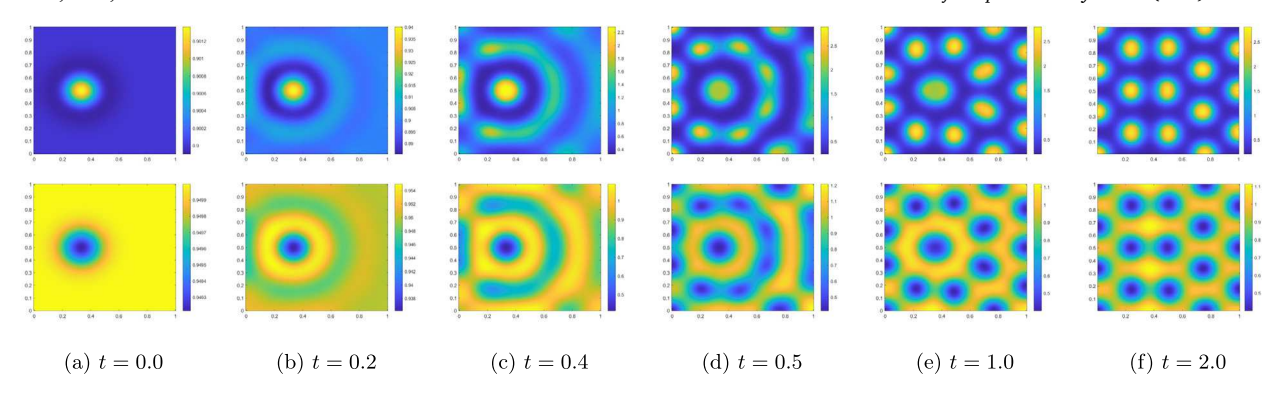


Fig. 10. Numerical solution of u (upper row), and v (lower row) at different time stages with initial condition (37).

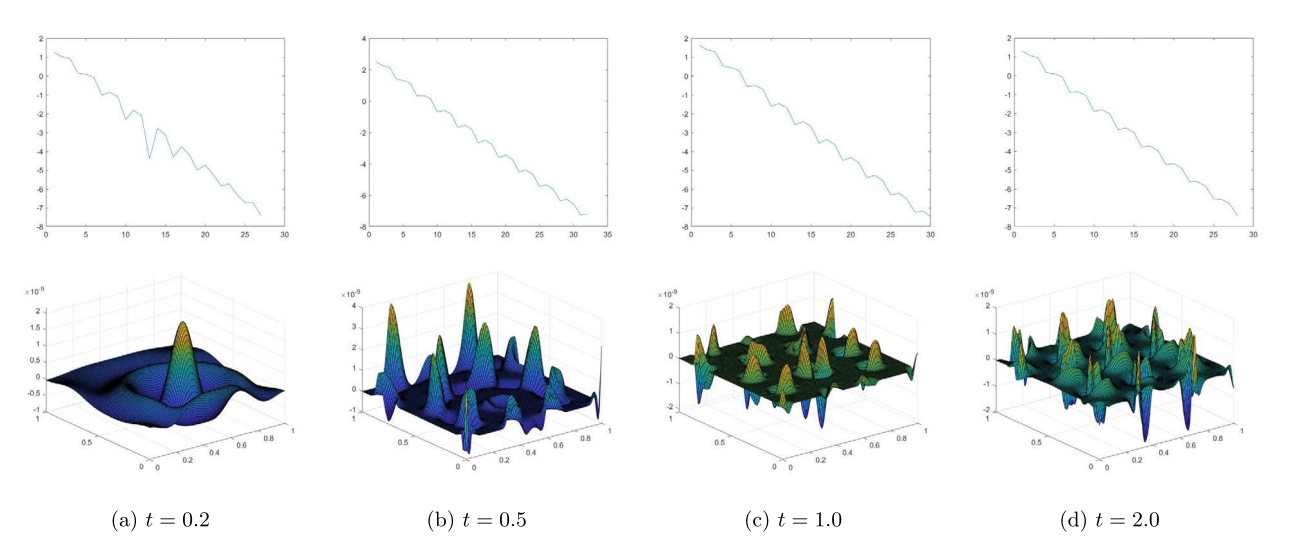


Fig. 11. The log-scaled residual decay of U and plots of residual Res(U) at different time stages t = 0.2, 0.5, 1.0, 2.0.

$$\begin{split} Q_{n+1} &= Q_n + \tau_p G_v^{-1}(V_n - V^k - h_t(D_2 \mathrm{Lap}_{h_x}^{\mathrm{N}} V_n + \kappa(b\mathbf{1} - U_n^2 \odot V_n))); \\ \widetilde{P}_{n+1} &= P_{n+1} + \omega(P_{n+1} - P_n); \quad \widetilde{Q}_{n+1} &= Q_{n+1} + \omega(Q_{n+1} - Q_n); \\ U_{n+1} &= U_n - \tau_u (\widetilde{P}_{n+1} - h_t(D_1 \mathrm{Lap}_{h_x}^{\mathrm{N}} \widetilde{P}_{n+1} + \kappa(-\widetilde{P}_{n+1} + 2U_n \odot V_n \odot (\widetilde{P}_{n+1} - \widetilde{Q}_{n+1}))). \\ V_{n+1} &= V_n - \tau_u (\widetilde{Q}_{n+1} - h_t(D_2 \mathrm{Lap}_{h_n}^{\mathrm{N}} \widetilde{Q}_{n+1} + \kappa(U_n^2 \odot (\widetilde{P}_{n+1} - \widetilde{Q}_{n+1}))). \end{split}$$

We recall that the Discrete Cosine Transform mentioned in Remark 1 can be used to compute matrix-vector multiplication involving  $\operatorname{Lap}_{h_x}^N$  as well as inverting the preconditioners  $G_u, G_v$  within  $O(N_x^2 \log N_x)$  complexity. Thus every step of the above PDHG iterations can be computed efficiently.

In our numerical implementation, we solve this PDE system, on time interval [0,2]. We choose  $N_x=128$ ,  $h_x=1/128$ ; and  $N_t=10000$ ,  $h_t=1/5000$ . We then choose  $\tau_u=\tau_p=0.9$ . We terminate the PDHG iteration when  $\|\mathrm{Res}(U_n)\|_2+\|\mathrm{Res}(V_n)\|_2<\delta$ , where we pick threshold  $\delta=10^{-7}$ . Our numerical solutions are presented in the following Fig. 10.

In this example, the performance of the PDHG method is stable and the method terminates in around 30 iterations for all 10000 time steps. We plot the loss as well as the residual term Res(U) at different time stages in Fig. 11.

We compare the computational speed of our PHDG method with the commonly used Newton-SOR method [45,34]. We fix all the parameters the same for both methods, typically, we set the termination threshold for both methods to be  $\delta=10^{-7}$ . We solve the PDE system on [0,1] with  $N_t=5000$  and  $N_x=128$ . The time cost for the Newton-SOR method is 8122.81s, while the time cost for the PDHG method is 1121.81s.

#### 4.4.2. Wolf-deer model

At last, let us consider an equation system describing the evolution of predator (wolves) and prey (deer) distributions in an ecology system [36,21]. The PDE system is defined on the region  $\Omega = [-L, L]^2$  and takes the following form,

$$\frac{\partial \rho_1}{\partial t} = D\Delta \rho_1 + \nabla \cdot (\rho_1 \nabla \mathcal{V}_1(\rho_1, \rho_2)) + A\rho_1 (1 - \rho_1) - B \frac{\rho_1 \rho_2}{1 + \rho_1}; \tag{38}$$

$$\frac{\partial \rho_2}{\partial t} = D\Delta \rho_2 + \nabla \cdot (\rho_2 \nabla \mathcal{V}_2(\rho_1, \rho_2)) + B \frac{\rho_1 \rho_2}{1 + \rho_1} - C\rho_2. \tag{39}$$

Here we set  $D = \frac{1}{2}$ , A = 5, B = 35,  $C = \frac{5}{2}$ . We also define the interacting potentials  $\mathcal{V}_1$ ,  $\mathcal{V}_2$  as

$$\mathcal{V}_1(\rho_a,\rho_b)(\cdot) = V*\rho_1 - V*\rho_2; \quad \mathcal{V}_2(\rho_a,\rho_b)(\cdot) = V*\rho_1 + V*\rho_2.$$

Here the convolution is defined as  $V*\rho(x,y)=\int_{\Omega\times\Omega}V((x,y)-(x',y'))\rho(x',y')~dx'dy'$  with potential  $V(x,y)=\frac{x^2+y^2}{2}$ . We choose Neumann boundary condition for both  $\rho_1$  and  $\rho_2$ , and set the initial condition

$$\rho_i(x,0) = \frac{1}{\pi} \left( \frac{\pi}{2} + \arctan\left(\frac{R^2 - |X - \vec{\mu}_i|^2}{\epsilon}\right) \right), \ i = 1, 2, \tag{40}$$

where  $\vec{\mu}_1 = (\frac{3}{2}, \frac{3}{2}), \ \vec{\mu}_2 = (-\frac{3}{2}, -\frac{3}{2}), \ R = 1 \text{ and } \epsilon = 0.1.$ 

In system (38), (39),  $\rho_1$  represents the distribution of deer, and  $\rho_2$  stands for the distribution of wolf. In addition to the diffusion and reaction terms affecting  $\rho_a$ ,  $\rho_2$ , the PDE system (38), (39) contain non-local drift terms  $\nabla \mathcal{V}_1(\rho_a, \rho_2)$ ,  $\nabla \mathcal{V}_2(\rho_1, \rho_2)$  that depict the interactions among the individuals of wolves and deer: The deer are attracting each other to dodge wolves' predation, while the wolves are gathering together to chase the flock of deer.

Suppose we discretize each side of  $\Omega$  into  $N_x - 1$  equal subintervals, we denote the numerical solutions at the *n*-th time step as  $\rho_1^n, \rho_2^n \in \mathbb{R}^{N_x^2}$ . We consider the following implicit, central-difference scheme,

$$\begin{split} \frac{\rho_1^{n+1}-\rho_1^n}{h_t} - D \mathrm{Lap}_{h_x}^\mathrm{N} \rho_1^{n+1} - D_x^\mathsf{T} (\overline{\rho_1^{n+1}}^x \odot D_x (K \rho_1^{n+1} - K \rho_2^{n+1})) \\ - D_y^\mathsf{T} (\overline{\rho_1^{n+1}}^y \odot D_y (K \rho_1^{n+1} - K \rho_2^{n+1})) + R_1 (\rho_1^{n+1}, \rho_2^{n+1}) = 0; \\ \frac{\rho_2^{n+1}-\rho_2^n}{h_t} - D \mathrm{Lap}_{h_x}^\mathrm{N} \rho_2^{n+1} - D_x^\mathsf{T} (\overline{\rho_2^{n+1}}^x \odot D_x (K \rho_1^{n+1} + K \rho_2^{n+1})) \\ - D_y^\mathsf{T} (\overline{\rho_2^{n+1}}^y \odot D_y (K \rho_1^{n+1} + K \rho_2^{n+1})) + R_2 (\rho_1^{n+1}, \rho_2^{n+1}) = 0. \end{split}$$

Here  $D_x$  is an  $(N_x+1)N_x\times N_x^2$  matrix which can be treated as the discrete gradient with respect to x, i.e., for any  $u\in\mathbb{R}^{N_x^2}$ ,  $(D_xu)_{(i,j+\frac{1}{2})}$  equals  $\frac{u_{i,j+1}-u_{i,j}}{h_x}$  for  $1\leq i\leq N_x$ ,  $1\leq j\leq N_x-1$ ; for  $j=0,N_x$ , we define  $(D_xu)_{(i,\frac{1}{2})}=\frac{u_{i,2}-u_{i,1}}{h_x}$  and  $(D_xu)_{(i,N_x+\frac{1}{2})}=\frac{u_{i,N_x}-u_{i,N_x-1}}{h_x}$ .  $D_y$  can also be defined in a similar way.

The notation  $\overline{\rho_1^{n+1}}^x \in \mathbb{R}^{(N_x+1)N_x}$  denotes the average value of  $\rho_1^{n+1}$  at midpoints, i.e.,  $(\overline{\rho_1^{n+1}}^x)_{(i,j+\frac{1}{2})} = \frac{\rho_{1,(i,j)}^{n+1} + \rho_{1,(i,j+1)}^{n+1}}{2}$  for  $1 \le i \le N_x$ ,  $1 \le j \le N_x - 1$ ; for j = 0,  $N_x$ , we define  $\overline{\rho_1^{n+1}}_{(i,\frac{1}{2})}^x = \rho_{1,i,1}^{n+1}$  and  $\overline{\rho_1^{n+1}}_{(i,N_x+\frac{1}{2})}^x = \rho_{1,N_x}^{n+1}$ .  $\overline{\rho_1^{n+1}}^y$ ,  $\overline{\rho_2^{n+1}}^x$ ,  $\overline{\rho_2^{n+1}}^y$  can be defined in the similar way.

*K* is an  $N_x^2 \times N_x^2$  matrix used for approximating the convolution  $V * \rho_1, V * \rho_2$ , to precisely, for any  $u \in \mathbb{R}^{N_x^2}$  defined on the mesh grid of  $\Omega$ , Ku is defined as

$$(Ku)_{(i,j)} = \sum_{1 \le k,l \le N_x} h_x^2 V(v_{i,j} - v_{k,l}) u_{k,l} = \sum_{1 \le k,l \le N_x} \frac{h_x^4}{2} ((i-k)^2 + (j-l)^2) u_{k,l}.$$

The above discrete convolution can be reduced to Toeplitz matrix-vector multiplication computation, which can be efficiently computed by FFT algorithm [47].

Furthermore, for  $\rho_1, \rho_2 \in \mathbb{R}^{N_x^2}$  the reaction terms are defined as  $R_1(\rho_1, \rho_2) = A\rho_1 \odot (1 - \rho_1) - B \frac{\rho_1}{1 + \rho_1} \odot \rho_2$ ;  $R_2(\rho_1, \rho_2) = B \frac{\rho_1}{1 + \rho_1} \odot \rho_2 - C\rho_2$ .

Given the above discrete scheme of the PDE system, similar to the discussion made in the Schnakenberg model, our purpose is to solve two nonlinear equations  $F_{\rho_1}(\rho_1,\rho_2)=0$ ,  $F_{\rho_2}(\rho_1,\rho_2)=0$  at each time step n. We apply two dual variables P,Q, and compose the corresponding PDHG dynamic for solving the two equations. According to the previous discussion, one can verify that each PDHG step can be computed within  $O(N_x^2 \log N_x)$  complexity. This guarantees the efficiency of the computation. To keep the discussion concise, we omit the exact formulas for the PDHG dynamic here.

In our implementation, we set L=3. We solve the equation system (38), (39) on time interval [0,1]. We set  $N_x=128$ ,  $h_x=3/64$ . We practice the method of adaptive time stepsize  $h_t$  in this example. We set both our initial time stepsize  $h_t$  and maximum stepsize  $h_t^0$  equal to 1/500 with shrinkage/enlarge coefficient  $\eta$  as 0.75. The thresholding iteration numbers of shrinking and enlarging  $h_t$  are set to be  $N^*=100$ , and  $N_*=20$ . For the PDHG iteration, we set stepsize  $\tau_u=\tau_p=0.95$ , and pick the threshold  $\delta=5\times 10^{-6}$ . We present the numerical results in Fig. 12.

The linear convergence of the residual term  $\|\text{Res}(U)\|_2$  is reflected from the residual decay plots in Fig. 13.

The changes in PDHG iterations at each time stepsize as well as the changes in time step size  $h_t$  are demonstrated via Fig. 14. As reflected from the plots, in this example, we are gradually shrinking the time stepsize  $h_t$  as the accumulated time increases to guarantee the computational efficiency of the PDHG method. Our method takes a total of 1106 time to complete the computation.

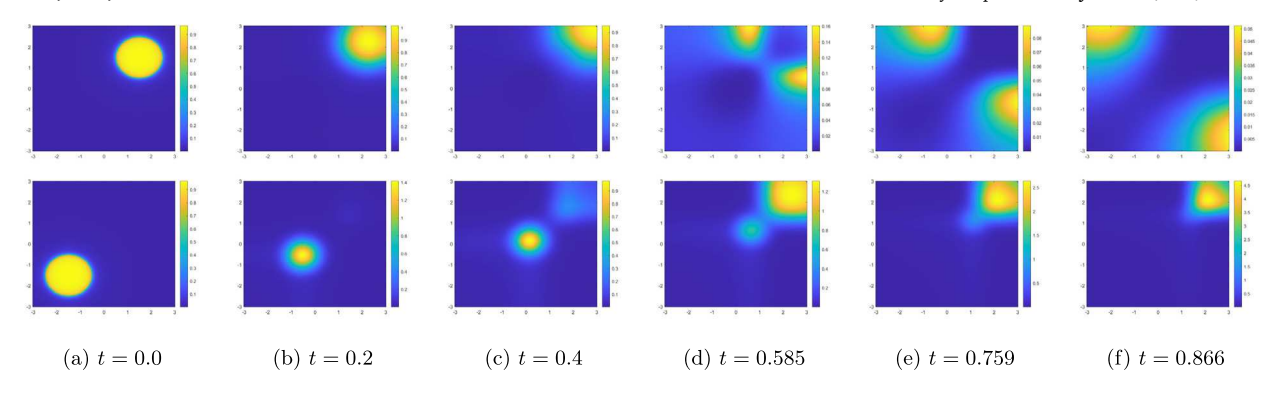


**Fig. 12.** Numerical solution of  $\rho_1$  (upper row), and  $\rho_2$  (lower row) at different time stages with initial condition (40).



**Fig. 13.** The log-scaled plot of  $Res(U_n)$  vs PDHG iteration number n at different time stages.

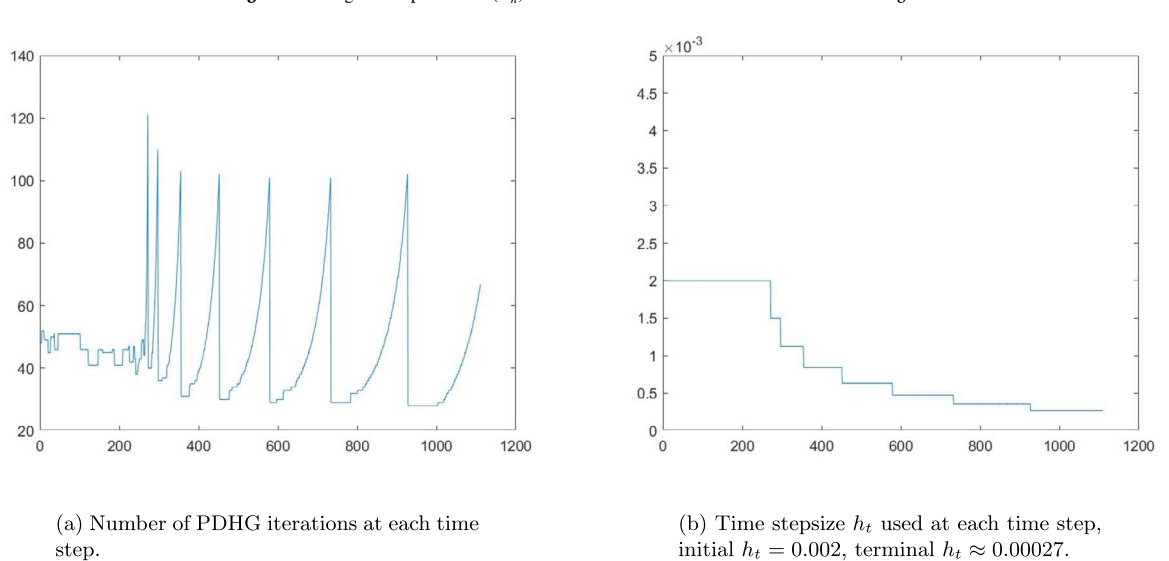


Fig. 14. Changes in number of PDHG iterations & time stepsize  $h_t$ .

The algorithm experiences 7 stepsize shrinkage among our computation. The initial  $h_t$  is set as 0.002 while when we finish the computation,  $h_t = 0.00027$ .

#### 5. Conclusion and future study

This research proposes an iterative method as a convenient but efficient gadget for solving the implicit (or semi-implicit) numerical schemes arising in time-evolution PDEs, especially the reaction-diffusion type equations. Our method recasts the nonlinear equation from the discrete numerical scheme at each time step as a min-max saddle point problem and applies the Primal-Dual Hybrid Gradient method. The algorithm can flexibly fit into various numerical schemes, such as semi-implicit and fully implicit schemes, etc. Furthermore, the method is easy to implement since it gets rid of the computation of large-scale linear systems involving Jacobian matrices, which are usually required by Newton's methods. The performance of our method on accuracy and efficiency is satisfying and is comparable to the commonly used Newton-type methods. This has been verified by the numerical examples presented in this paper.

There are four main future research directions of our work. We summarize them below:

- As mentioned in [32], it is appealing to solve the numerical solution of a time-evolution PDE on multiple time steps in a single run of the PDHG algorithm. We plan to extend the G-prox PDHG algorithm to the multi-step case by designing an efficient preconditioner, and then compare the efficiency between the two algorithms.
- Conduct the theoretical study on the proposed PDHG method when applied to RD-type equations. There are two aspects of the theory: (1) Determine the conditions on  $h_x$ ,  $h_t$  under which the implicit scheme admits a unique solution. Some related work has already been done in [50]; (2) Determine the conditions on  $h_x$ ,  $h_t$ , as well as the parameters  $\tau_u$ ,  $\tau_p$  and  $\omega$  under which the proposed PDHG method is guaranteed to converge.
- Generalize the method to nonlinear time-evolution equations, especially the advection-reaction-diffusion dynamics from GENERIC (General Equation for Non-Equilibrium Reversible-Irreversible Coupling) [17,24,37].
- · Apply the method to high-dimensional time-evolution PDEs by leveraging deep learning techniques and PDHG algorithms.

#### CRediT authorship contribution statement

**Shu Liu:** Conceptualization, Methodology, Software, Writing – original draft, Writing – review & editing. **Siting Liu:** Conceptualization, Methodology, Writing – original draft, Writing – review & editing. **Stanley Osher:** Conceptualization, Methodology, Writing – original draft, Writing – review & editing. **Wuchen Li:** Conceptualization, Methodology, Writing – original draft, Writing – review & editing.

#### **Declaration of competing interest**

The authors declare that they have no known competing financial interests or personal relationships that could have appeared to influence the work reported in this paper.

#### Data availability

Data will be made available on request.

#### Acknowledgement

S. Liu, S. Liu, and S. Osher's work was partly supported by AFOSR MURI FP 9550-18-1-502 and ONR grants: N00014-20-1-2093 and N00014-20-1-2787. W. Li's work was supported by AFOSR MURI FP 9550-18-1-502, AFOSR YIP award No. FA9550-23-1-0087, and NSF RTG: 2038080.

#### Appendix A. Proof of Theorem 1

**Proof.** It is not hard to verify that the dynamic (14), (15) and (17) can be formulated as

$$\begin{bmatrix} U_{n+1} \\ P_{n+1} \end{bmatrix} = \begin{bmatrix} I - 2\tau_u \tau_p A^\top A & -\tau_u A^\top \\ \tau_p A & I \end{bmatrix} \begin{bmatrix} U_n \\ P_n \end{bmatrix} + \begin{bmatrix} 2\tau_u \tau_p A^\top b \\ -\tau_p b \end{bmatrix}, \quad n \ge 0$$

$$\tag{41}$$

This equation admits a unique fixed point  $X_* = (U_*, P_*) = (A^{-1}b, 0)$ . We denote  $X_n = [U_n^\top, P_n^\top]^\top$  and the above recurrence equation as  $X_{n+1} = MX_n + y$  (or equivalently,  $X_{n+1} - X_* = M(X_n - X_*)$ ) for shorthand. Suppose A has spectral decomposition  $A = Q\Lambda Q^\top$ , then M is decomposed as

$$M = \left[ \begin{array}{cc} Q & \\ & Q \end{array} \right] \left[ \begin{array}{cc} I - 2\tau_u\tau_p\Lambda^2 & -\tau_u\Lambda \\ & \tau_p\Lambda & I \end{array} \right] \left[ \begin{array}{cc} Q & \\ & Q \end{array} \right]^\top$$

We denote  $N_A$  as the size of A. The middle matrix is composed of four  $N_A \times N_A$  diagonal matrices, by rearranging the rows and columns of it, one can show that it is orthogonally equivalent to the block diagonal matrix  $\Sigma = \text{diag}(D_1, D_2, ..., D_{N_A})$  where each

$$D_k = \begin{bmatrix} 1 - 2\tau_u\tau_p\lambda_k^2 & -\tau_u\lambda_k \\ \tau_p\lambda_k & 1 \end{bmatrix}. \text{ We now analyze the spectral radius } \rho(M) \text{ of } M, \text{ which equals } \rho(\Sigma) = \max_{1 \leq k \leq N_A} \{\rho(D_k)\}. \text{ We can calculate } \rho(D_k) = \sum_{k \leq N_A} \{\rho(D_k)\}.$$

$$\rho(D_k) = \max\{|\tau_u \tau_p \lambda_k^2 - 1 \pm \sqrt{(\tau_u \tau_p)^2 \lambda_k^4 - \tau_u \tau_p \lambda_k^2}|\}.$$

We denote  $f(t) = \max\{|t - 1 + \sqrt{t^2 - t}|, |t - 1 - \sqrt{t^2 - t}|\}$ , with t > 0. One can directly compute  $f(t) = \begin{cases} \sqrt{1 - t} & 0 < t \le 1 \\ t - 1 + \sqrt{t^2 - t} & t > 1 \end{cases}$ 

Thus we have  $\rho(M) = \max_{1 \le k \le N_A} \{f(\tau_u \tau_p \lambda_k^2)\}$ . Then f is decreasing on [0,1] and increasing on  $[1,\infty)$  with  $f(0) = f(\frac{4}{3}) = 1$ . We know that the convergence of (41) is guaranteed if and only if  $\rho(M) < 1$ . This is equivalent to  $\tau_u \tau_p \lambda_{\max}^2 \le \frac{4}{3}$ , which yields  $\tau_u \tau_p \le \frac{4}{3\lambda_{\max}^2}$ .

Furthermore,  $\rho(M)$  is the convergence rate of the dynamic, i.e.,

$$||X_n - X_*||_2 \le \rho(M)^n ||X_0 - X_*||_2$$

To evaluate the optimal convergence rate, we compute the minimum value of  $\rho(M)$  w.r.t. stepsizes  $\tau_u, \tau_p$ . Suppose we require  $\tau_u \tau_p \leq \frac{4}{3\lambda_{\max}^2}$  to guarantee convergence, if we denote  $\eta = \tau_u \tau_p \lambda_{\max}^2$ , then  $\rho(M) = \max_{1 \leq k \leq N_A} \left\{ f(\frac{\lambda_k^2}{\lambda_{\max}^2} \eta) \right\}$  for  $\eta \in (0, \frac{4}{3})$ . The minimum value of  $\rho(M)$  will be attained at a unique  $\eta = \eta_* \in [1, \frac{4}{3})$  such that  $f(\frac{\eta}{v^2}) = f(\eta)$ . I.e.,  $\eta^*$  is the solution of

$$\sqrt{1 - \frac{\eta}{\kappa^2}} = \eta - 1 + \sqrt{\eta^2 - \eta}, \quad \text{on } [1, \frac{4}{3}). \tag{42}$$

Thus, the optimal convergence rate  $\gamma_* = \sqrt{1 - \frac{\eta_*}{\kappa^2}}$  and it is achieved when  $\tau_u, \tau_p$  satisfy  $\tau_u \tau_p = \frac{\eta^*}{\lambda_{\max}^2}$ .

**Remark 2.** The equation (42) can be reduced to a quadratic equation. And it admits a unique solution  $\eta_*$  on  $[1, \frac{4}{3})$ ,  $\eta_*$  takes the following form

$$\eta_* = \frac{2\kappa^2}{\left(\frac{3}{4}\kappa^2 + \frac{3}{2} - \frac{1}{4\kappa^2}\right) + \frac{\kappa - 1}{2\kappa}\sqrt{(\kappa - 1)(3\kappa + 1)}\sqrt{\frac{3}{4}\kappa^2 + \frac{3}{2} + 2\kappa - \frac{1}{4\kappa^2}}}.$$

The optimal convergence rate  $\gamma_* = \sqrt{1 - \frac{\eta_*}{\kappa^2}}$  takes the explicit form

$$\gamma_* = \left(1 - \frac{2}{\left(\frac{3}{4}\kappa^2 + \frac{3}{2} - \frac{1}{4\kappa^2}\right) + \frac{\kappa - 1}{2\kappa}\sqrt{(\kappa - 1)(3\kappa + 1)}\sqrt{\frac{3}{4}\kappa^2 + \frac{3}{2} + 2\kappa - \frac{1}{4\kappa^2}}}\right)^{\frac{1}{2}}.$$

Notice that  $\gamma_* \approx (1 - \frac{4}{3\kappa^2})^{\frac{1}{2}}$  when the conditional number  $\kappa$  is very large; and  $\gamma_*$  will approach 0 as condition number  $\kappa$  approaches 1. This motivates the preconditioning technique of our method.

#### References

- [1] Samuel M. Allen, John W. Cahn, A microscopic theory for antiphase boundary motion and its application to antiphase domain coarsening, Acta Metall. 27 (6) (1979) 1085–1095.
- [2] Sokratis J. Anagnostopoulos, Juan Diego Toscano, Nikolaos Stergiopulos, George Em Karniadakis, Residual-based attention and connection to information bottleneck theory in pinns, arXiv preprint arXiv:2307.00379, 2023.
- [3] Kendall Atkinson, An Introduction to Numerical Analysis, John Wiley & Sons, 1991.
- [4] Gang Bao, Xiaojing Ye, Yaohua Zang, Haomin Zhou, Numerical solution of inverse problems by weak adversarial networks, Inverse Probl. 36 (11) (2020) 115003.
- [5] John W. Cahn, On spinodal decomposition, Acta Metall. 9 (9) (1961) 795-801.
- [6] José A. Carrillo, Katy Craig, Li Wang, Chaozhen Wei, Primal dual methods for Wasserstein gradient flows, Found. Comput. Math. 22 (2) (2022) 389-443.
- [7] Jose A. Carrillo, Li Wang, Chaozhen Wei, Structure Preserving Primal Dual Methods for Gradient Flows with Nonlinear Mobility Transport Distances, 2023.
- [8] Hector D. Ceniceros, Carlos J. García-Cervera, A new approach for the numerical solution of diffusion equations with variable and degenerate mobility, J. Comput. Phys. 246 (2013) 1–10.
- [9] Antonin Chambolle, Thomas Pock, A first-order primal-dual algorithm for convex problems with applications to imaging, J. Math. Imaging Vis. 40 (2011)
- [10] Long Chen, Jingrong Wei, Accelerated gradient and skew-symmetric splitting methods for a class of monotone operator equations, arXiv preprint arXiv:2303.
- [11] Long Chen, Jingrong Wei, Transformed primal-dual methods for nonlinear saddle point systems, J. Numer. Math. (2023).
- [12] Ching-Shan Chou, Yong-Tao Zhang, Rui Zhao, Qing Nie, Numerical methods for stiff reaction-diffusion systems, Discrete Contin. Dyn. Syst., Ser. B 7 (3) (2007) 515.
- [13] Andrew Christlieb, Jaylan Jones, Keith Promislow, Brian Wetton, Mark Willoughby, High accuracy solutions to energy gradient flows from material science models, J. Comput. Phys. 257 (2014) 193–215.
- [14] Jon M. Church, Zhenlin Guo, Peter K. Jimack, Anotida Madzvamuse, Keith Promislow, Brian Wetton, Steven M. Wise, Fengwei Yang, High accuracy benchmark problems for Allen-Cahn and Cahn-Hilliard dynamics, Commun. Comput. Phys. 26 (4) (2019).
- [15] Christian Clason, Tuomo Valkonen, Primal-dual extragradient methods for nonlinear nonsmooth PDE-constrained optimization, SIAM J. Optim. 27 (3) (2017) 1314–1339.
- [16] Richard Courant, Kurt Friedrichs, Hans Lewy, Über die partiellen Differenzengleichungen der mathematischen Physik, Math. Ann. 100 (1) (1928) 32–74.
- [17] Manh Hong Duong, Michela Ottobre, Non-reversible processes: GENERIC, hypocoercivity and fluctuations, Nonlinearity 36 (3) (2023) 1617.
- [18] David J. Eyre, An unconditionally stable one-step scheme for gradient systems, Unpubl. Artic. (1998) 6.
- [19] Fariba Fahroo, Kazufumi Ito, Optimum damping design for an abstract wave equation, Kybernetika 32 (6) (1996) 557-574.
- [20] Guosheng Fu, Stanley Osher, Wuchen Li, High order spatial discretization for variational time implicit schemes: Wasserstein gradient flows and reaction-diffusion systems, arXiv preprint arXiv:2303.08950, 2023.
- [21] Thomas Gallouët, Maxime Laborde, Leonard Monsaingeon, An unbalanced optimal transport splitting scheme for general advection-reaction-diffusion problems, ESAIM Control Optim. Calc. Var. 25 (8) (2019).
- [22] Nir Gavish, Jaylan Jones, Zhengfu Xu, Andrew Christlieb, Keith Promislow, Variational models of network formation and ion transport: applications to perfluorosulfonate ionomer membranes. Polymers 4 (1) (2012) 630–655.

- [23] Gene H. Golub, Charles F. Van Loan, Matrix Computations, JHU Press, 2013.
- [24] Miroslav Grmela, Hans Christian Öttinger, Dynamics and thermodynamics of complex fluids. I. Development of a general formalism, Phys. Rev. E 56 (6) (1997) 6620.
- [25] Willem H. Hundsdorfer, Jan G. Verwer, W.H. Hundsdorfer, Numerical Solution of Time-Dependent Advection-Diffusion-Reaction Equations, vol. 33, Springer, 2003
- [26] Matt Jacobs, Flavien Léger, Wuchen Li, Stanley Osher, Solving large-scale optimization problems with a convergence rate independent of grid size, SIAM J. Numer. Anal. 57 (3) (2019) 1100–1123.
- [27] Andrea M. Jokisaari, P.W. Voorhees, Jonathan E. Guyer, James Warren, O.G. Heinonen, Benchmark problems for numerical implementations of phase field models. Comput. Mater. Sci. 126 (2017) 139–151.
- [28] Yibao Li, Hyun Geun Lee, Darae Jeong, Junseok Kim, An unconditionally stable hybrid numerical method for solving the Allen-Cahn equation, Comput. Math. Appl. 60 (6) (2010) 1591–1606.
- [29] Chun Liu, Cheng Wang, Yiwei Wang, A structure-preserving, operator splitting scheme for reaction-diffusion equations with detailed balance, J. Comput. Phys. 436 (2021) 110253.
- [30] Chun Liu, Cheng Wang, Yiwei Wang, A second-order accurate, operator splitting scheme for reaction-diffusion systems in an energetic variational formulation, SIAM J. Sci. Comput. 44 (4) (2022) A2276–A2301.
- [31] Chun Liu, Cheng Wang, Yiwei Wang, Steven M. Wise, Convergence analysis of the variational operator splitting scheme for a reaction-diffusion system with detailed balance, SIAM J. Numer. Anal. 60 (2) (2022) 781–803.
- [32] Siting Liu, Stanley Osher, Wuchen Li, Chi-Wang Shu, A primal-dual approach for solving conservation laws with implicit in time approximations, J. Comput. Phys. 472 (2023).
- [33] Levi McClenny, Ulisses Braga-Neto, Self-adaptive physics-informed neural networks using a soft attention mechanism, arXiv preprint arXiv:2009.04544, 2020.
- [34] Barry Merriman, James K. Bence, Stanley J. Osher, Motion of multiple junctions: a level set approach, J. Comput. Phys. 112 (2) (1994) 334-363.
- [35] Barry Merriman, James Kenyard Bence, Stanley Osher, Diffusion Generated Motion by Mean Curvature, Department of Mathematics, University of California, Los Angeles, 1992.
- [36] James D. Murray, Mathematical Biology II: Spatial Models and Biomedical Applications, vol. 3, Springer, New York, 2001.
- [37] Hans Christian Öttinger, Miroslav Grmela, Dynamics and thermodynamics of complex fluids. II. Illustrations of a general formalism, Phys. Rev. E 56 (6) (1997) 6633
- [38] Lorenzo Pareschi, Giovanni Russo, Implicit-explicit Runge-Kutta schemes for stiff systems, Recent Trends Numer. Anal. 3 (2000) 269.
- [39] John E. Pearson, Complex patterns in a simple system, Science 261 (5118) (1993) 189-192.
- [40] Jacob Rubinstein, Peter Sternberg, Joseph B. Keller, Fast reaction, slow diffusion, and curve shortening, SIAM J. Appl. Math. 49 (1) (1989) 116-133.
- [41] J. Schnakenberg, Simple chemical reaction systems with limit cycle behaviour, J. Theor. Biol. 81 (3) (1979) 389-400.
- [42] Jie Shen, Jie Xu, Jiang Yang, The scalar auxiliary variable (SAV) approach for gradient flows, J. Comput. Phys. 353 (2018) 407-416.
- [43] Jie Shen, Jie Xu, Jiang Yang, A new class of efficient and robust energy stable schemes for gradient flows, SIAM Rev. 61 (3) (2019) 474-506.
- [44] Jie Shen, Xiaofeng Yang, Numerical approximations of Allen-Cahn and Cahn-Hilliard equations, Discrete Contin. Dyn. Syst. 28 (4) (2010) 1669–1691.
- [45] Andrew H. Sherman, On Newton-iterative methods for the solution of systems of nonlinear equations, SIAM J. Numer. Anal. 15 (4) (1978) 755–771.
- [46] Martin B. Short, P. Jeffrey Brantingham, Andrea L. Bertozzi, George E. Tita, Dissipation and displacement of hotspots in reaction-diffusion models of crime, Proc. Natl. Acad. Sci. 107 (9) (2010) 3961–3965.
- [47] Gilbert Strang, A proposal for Toeplitz matrix calculations, Stud. Appl. Math. 74 (2) (1986) 171–176.
- [48] Gilbert Strang, The discrete cosine transform, SIAM Rev. 41 (1) (1999) 135-147.
- [49] Tuomo Valkonen, A primal-dual hybrid gradient method for nonlinear operators with applications to MRI, Inverse Probl. 30 (5) (2014) 055012.
- [50] Jinchao Xu, Yukun Li, Shuonan Wu, Arthur Bousquet, On the stability and accuracy of partially and fully implicit schemes for phase field modeling, Comput. Methods Appl. Mech. Eng. 345 (2019) 826–853.
- [51] Xiaofeng Yang, Linear first and second-order, unconditionally energy stable numerical schemes for the phase field model of homopolymer blends, J. Comput. Phys. 327 (2016) 294–316.
- [52] Yaohua Zang, Gang Bao, Xiaojing Ye, Haomin Zhou, Weak adversarial networks for high-dimensional partial differential equations, J. Comput. Phys. 411 (2020) 109409.
- [53] Jianfeng Zhu, Yong-Tao Zhang, Stuart A. Newman, Mark Alber, Application of discontinuous Galerkin methods for reaction-diffusion systems in developmental biology, J. Sci. Comput. 40 (2009) 391–418.
- [54] Mingqiang Zhu, Tony Chan, An efficient primal-dual hybrid gradient algorithm for total variation image restoration, UCLA CAM Rep. 34 (2008) 8-34.